Extensive Intratumor Proteogenomic Heterogeneity Revealed by Multiregion Sampling in High-Grade Serous Ovarian Tumor Specimens

Allison L. Hunt[1,2^], Nicholas W. Bateman[2-4^], Waleed Barakat[2,3], Sasha Makohon-Moore[2,3], Brian L. Hood[2,3], Kelly A. Conrads[2,3], Ming Zhou[1,2], Valerie Calvert[5], Mariaelena Pierobon[5], Jeremy Loffredo[2,3], Tracy J. Litzi[2,3], Julie Oliver[2,3], Dave Mitchell[2,3], Glenn Gist[2,3], Christine Rojas[2], Brian Blanton[2,4], Emma L. Robinson[1,2], Kunle Odunsi[6], Anil K. Sood[7], Yovanni Casablanca[2-4], Kathleen M. Darcy[2-4], Craig D. Shriver[4], Emanuel F. Petricoin[5], Uma N. M. Rao[2,3†], G. Larry Maxwell[1,2,4*] and Thomas P. Conrads[1,2,4*]

[1]Women's Health Integrated Research Center, Inova Women's Service Line, Inova Health System, 3289 Woodburn Rd, Annandale, VA 22042, USA.

[2]Gynecologic Cancer Center of Excellence, Department of Obstetrics and Gynecology, Uniformed Services University and Walter Reed National Military Medical Center, 8901 Wisconsin Avenue, Bethesda 20889, MD, USA.

[3]The Henry M. Jackson Foundation for the Advancement of Military Medicine, Inc., 6720A Rockledge Drive, Suite 100, Bethesda, MD 20817.

[4]The John P. Murtha Cancer Center Research Program, Department of Surgery, Uniformed Services University, 8901 Wisconsin Avenue, Bethesda 20889, MD, USA.

[5]Center for Applied Proteomics and Molecular Medicine, George Mason University, Manassas, VA

[6]Department of Gynecologic Oncology, Roswell Park Comprehensive Cancer Center, Buffalo, NY, 14263, USA.

[7]Department of Gynecologic Oncology and Reproductive Medicine, The University of Texas MD Anderson Cancer Center, Houston, TX, USA.

^Author's contributed equally to this work

[†] Dr. Uma NM Rao sadly passed away during the preparation of this manuscript

Running Title: Intratumor proteogenomic heterogeneity

Address correspondence to: Dr. Thomas P. Conrads (thomas.conrads@inova.org), 3289 Woodburn Rd, Suite 375, Annandale, VA, 22003, or Dr. G. Larry Maxwell (george.maxwell@inova.org), 3300 Gallows Road, Falls Church, VA, 22042.

Abstract

Enriched tumor epithelium, tumor-associated stroma, and whole tissue were collected by laser microdissection from thin sections across spatially separated levels of ten primary high-grade serous ovarian tumors and analyzed using proteomics (mass spectrometry and reverse phase protein microarray) and RNA-sequencing analyses. Comparative analyses of transcript and protein abundances revealed independent clustering of enriched stroma and enriched tumor epithelium, with whole tumor tissue clustering between purified collections, driven by overall tumor purity. Comparison of historic prognostic molecular subtypes for HGSOC revealed protein and transcript expression from tumor epithelium correlated most strongly with the differentiated molecular subtype, whereas stromal proteins and transcripts most strongly correlated with mesenchymal subtype. Protein and transcript abundance in tumor epithelium and stromal collections from neighboring sections exhibited decreased correlation in samples collected just hundreds of microns apart. These data reveal substantial protein and transcript expression heterogeneity within the tumor microenvironment that directly bears on prognostic signatures and underscore the need to enrich cellular subpopulations for expression profiling.

Introduction

Ovarian cancer is the fifth leading cause of death in women in the U.S. [1], with nearly 22,000 new cases and 14,000 deaths projected to occur in 2020. Most ovarian cancer cases are diagnosed at an advanced stage and exhibit heterogeneous populations and subpopulations of tumor cells that limit successful therapeutic intervention. The 5-year survival rate of patients diagnosed with metastatic ovarian cancer is less than 30% [2].

Numerous high-throughput sequencing studies aimed at broadly characterizing the genomic landscape of specific cancer types have been or are being conducted [3]. Although adding substantially to our molecular understanding of cancer, these studies have resulted in limited clinical translation, due in part to an ever increasing body of evidence that points to previously underappreciated levels of heterogeneity in the tumor microenvironment (TME) [4].

Substantial molecular and pathologic intra-tumoral differences in HGSOC tumors and their relationship with TME dynamics have been described [5, 6]. One study demonstrated that stable and/or regressing tumors lacked common neoepitopes and mutations compared to progressing tumors in the same patient [5], implicating non-somatic factors within the TME as critical determinants of immune response and overall tumor fate. Multiregional sampling has revealed extensive variation between subpopulations of cells within a single tumor [7-9], suggesting individual tumor samples have multiple subtype signatures present with differing levels of activation [10]. Single-cell RNA-seq of HGSOC samples has revealed grade-specific and cell type-specific transcriptional profiles representative of discrete cell types, such as tumor epithelium, stromal, and immune cells present within individual tumor specimens [7]. Further, the presence of subclonal cell populations within primary and/or metastatic tumors has been demonstrated to influence the state of immune infiltration and activation [8].

In this study, we investigated proteomic and transcriptomic heterogeneity in the TME from HGSOC patient primary tumors using laser microdissection (LMD) of spatially separated tumor enriched regions, stromal cell populations, as well as whole tumor collections throughout distinct levels from each specimen block. These results reveal stark molecular heterogeneity in the HGSOC tumor microenvironment and underscore the need to account for compartmental heterogeneity in the TME in molecular profiling analyses of HGSOC.

Results

Proteogenomic analyses of discrete cellular populations within a single HGSOC tumor using locoregional multi-sampling

Consecutive thin sections (~200) were generated from fresh-frozen primary HGSOC tumors (n=10 patients) to support multi-region sampling by LMD followed by integrated quantitative proteomic and transcriptomic analyses (Fig. 1A; Supplemental Fig. 1). All patients had advanced stage (stage III or IV) ovarian or tubo-ovarian disease (Supplemental Table 1). Primary specimens were obtained from ovarian and/or tubo-ovarian tissue and other pelvic masses, to include omentum. Some of the patients were chemotherapy-naïve (n=6) at the time of surgical resection, while others had received neoadjuvant chemotherapy (n=4). Representative hematoxylin and eosin (H&E) stained sections were reviewed by a board-certified pathologist (UNMR) to confirm histologic characteristics and tumor cellularity within each level (Supplemental Table 1).

Enriched tumor epithelium, stromal cells, as well as whole tumor collections representing all material on a single tissue section, were collected at spatially distinct intervals ("levels") from alternating sections throughout the tumor blocks (Fig. 1B; Supplemental Table 2). In case

101 343WM, additional LMD collections were conducted to generate spatially separated "cores"
102 (with additional technical replicate "cores") representing defined sub-populations of tumor
103 epithelium from alternating tissue sections that spanned the entirety of the patient tumor block
104 from four spatially diverse quadrants (i.e., 1 - 4) and combined into four independent sample
105 sets, including close biological collection "replicates" (i.e. 1A, 1B, 2A, 2B, etc) to support
106 comparative proteome and transcriptome analyses (Fig. 1B). Representative PEN membrane
107 slides after LMD were imaged, along with adjacent H&E stained tissue sections, to enable co-
108 registration and automated quantification of tumor and stromal cell populations collected
109 (Supplemental Table 3). There was marked discrepancy regarding estimation of tumor purity
110 between the automated and manual evaluations. Digital analysis estimated 23 - 56% tumor
111 cellularity at different depths of the block, calculated based on tumor regions of interest (ROI)
112 collected by LMD / whole tissue area (Supplemental Table 3). Further, automated estimates
113 revealed median cell number per area to be approximately 7,482 cells/mm^2. By cell type, this
114 represents an average of 7,527 ± 172 tumor cells (n=15 protein and RNA collections) or 3,899 ±
115 263 stroma cells (n=6 protein and RNA collections) collected by LMD per mm^2 of tissue area.
116 Comparatively, manual review estimated 75 - 95% tumor cellularity (Supplemental Table 1).
117 Differences between automated and manual review of tumor cellularity can likely be attributed
118 to the presence of small regions of interceding stroma and other cell types in and around the
119 tumor epithelium, which were excluded from the LMD tumor epithelium collections.

120 Multiregion protein samples were analyzed by mass spectrometry-based quantitative
121 proteomics using a multiplexed, isobaric tagging methodology (tandem mass tags, TMT-10 or
122 TMTpro-16; Supplemental Table 4) and reverse phase protein microarray (RPPA). RNA samples
123 were analyzed by targeted RNA-seq analyses. For 343WM, a total of 6,053 proteins

(Supplemental Table 5) and 20,535 transcripts (Supplemental Table 6) were quantified across all samples. For the remaining 9 cases, an average of 9,223 ± 511 proteins were measured within each patient-specific TMT plex for a total of 6,199 proteins co-quantified across all patients (Supplemental Table 7). A total of 19,758 transcripts were quantified from 343WB and 343WH (Supplemental Table 8).

Tumor and stromal cell populations exhibit diverse proteogenomic profiles

Unsupervised hierarchical cluster analysis of differentially expressed proteins (Supplemental Table 9) or transcripts (Supplemental Table 10) from case 343WM revealed distinct sub-clustering of tumor cores, enriched tumor epithelium and stroma, as well as whole tumor collections (Fig. 2A and B). Two predominant clusters stratifying tumor cores and tumor epithelium from stroma and whole tumor collections are apparent. Notably, the cryopulverized tissue proteome exhibited an intermediate cluster between these two sample groups (Fig. 2A), suggesting this sample type represents a mixture of these cellular populations. The proteins measured in the cryopulverized tissue also reflect contributions from the inclusion of blood, necrosis, and fat within this sample, which had been excluded from the whole tumor collections.

Similar clustering was seen across the additional 9 HGSOC patient tissue cell type collections; unsupervised hierarchical cluster analysis of proteins (Supplemental Table 11) and transcripts (Supplemental Table 12) revealed distinct clustering of the LMD enriched tumor epithelium from the LMD enriched stroma (Fig. 2C; Supplemental Fig. 2). Importantly, the extent to which the whole tumor tissue collection more closely associated with tumor epithelium or stroma was directly related to the tumor "purity" reflecting levels of overall tumor purity; namely, whole tumor tissues with high percent tumor epithelium associated with the LMD

147 enriched tumor epithelium and those with low percent tumor epithelium more strongly associated
148 with LMD enriched stroma (Supplemental Table 1).

149 We next examined the abundance of representative epithelial markers Ovarian Cancer-
150 Related Tumor Marker CA125/Mucin-16 (CA-125/*MUC16*), Keratin Type I Cytoskeletal 19
151 (*KRT19*), and Cadherin 1 (*CDH1*), and stromal markers Versican (VCAN) and Fibroblast
152 Activation Protein Alpha (FAP) across each tissue collection type (Fig. 3A). As expected,
153 MUC16 and CDH1 protein and transcript levels were more abundant in tumor cores and LMD
154 enriched tumor epithelial collections, and comparatively decreased in LMD enriched stroma and
155 whole tumor collections. VCAN and FAP abundance, in contrast, were elevated in LMD
156 enriched stroma and whole tumor collections, consistent with these proteins being stromal in
157 origin [11, 12]. Cell type enrichment analyses using transcript expression-level data from
158 343WM was performed (Supplemental Table 13) [13], and except for Cores 4A/B, all of the
159 LMD tumor cores and LMD enriched tumor epithelium collections correlated most strongly with
160 epithelial cell signatures, while the LMD enriched stroma and whole tumor collections had the
161 highest correlation with fibroblast cell signatures, stroma, as well as microenvironment scores
162 (Fig. 3A). Overall, these highly significant ($p<0.0001$) associations between epithelial and
163 stromal marker proteins KRT19, CDH1, VCAN, and FAP with LMD enriched tumor epithelium
164 and stroma, respectively, were observed in the additional 9 HGSOC cases assessed (Fig. 3B).
165 Cellular type enrichment scores were also significantly different in the additional 9 cases, in
166 which LMD enriched tumor was again significantly enriched for epithelial cells, while LMD
167 enriched stroma had the highest scores for fibroblasts, stroma, and microenvironment ($p<0.0001$;
168 Fig. 3C; Supplemental Table 14).

169 Notably, the abundance of MUC16 was not significantly different between LMD
170 enriched tumor and stroma (p=0.0825; Supplemental Fig. 3) in the proteomic datasets of the
171 additional 9 patients. MUC16 was elevated in LMD enriched stroma for cases 343VT and
172 343WQ and was not measured in any tissue collections from cases 343WH and 343WN. CA-125
173 is monitored as a clinical biomarker in serum for ovarian cancer progression and regression [14-
174 16] and is an epitope of the extracellular domain of the MUC16 protein [17-19] which can be
175 shed from HGSOC cells via proteolytic cleavage [20]. As MUC16 was not significantly altered
176 between LMD enriched tumor and stroma, we hypothesized the abundance of proteins shed or
177 secreted from tumor cells may exhibit greater variability within the tumor microenvironment due
178 to circulation within interstitial spaces as well as local vasculature. We therefore compared
179 abundance trends of proteins exhibiting a signal peptide sequence for targeting a protein for
180 secretion to the extracellular space, or that are characterized as being extracellular by Gene
181 Ontology, relative to proteins lacking these features across all collection levels to measure
182 whether the variance in protein abundance across levels was higher in proteins with versus
183 without signal peptides or extracellular localization. Cases 343WM, 343WK, 343WQ, and
184 343WH were selected for this analysis as proteomic data from all levels/case of each LMD
185 enriched tumor and stroma was available. We found that proteins with signal peptide sequences
186 expressed in the LMD enriched tumor epithelium in three cases and proteins in the LMD
187 enriched stroma from all four cases had significantly higher variance ($p<0.0001$) than proteins
188 lacking these sequences (Supplemental Table 15). Further, the variance of extracellular proteins
189 was also significantly higher ($p<0.001$) than those lacking this classification.

190 Integrated analyses of protein and transcript level data revealed 5,742 co-quantified
191 proteins and transcripts from 343WM across all tissue types (Fig. 4; Supplemental Table 16).

192 Proteins and their transcripts for a given LMD collection type showed positive correlation with
193 other samples from the same LMD collection type (e.g. Core 1A protein clustered most strongly
194 to its corresponding transcript and next nearest to other core collections). Notably, stromal
195 transcripts clustered most strongly with their cognate proteins from the whole tumor collections.
196 In comparison of replicate tumor cores, the strongest correlations, apart from intra-core
197 comparisons, were between the "A" and "B" replicates for each core. The A and B replicates for
198 each core at the proteome-only and transcriptome-only levels had Spearman Rho between 0.65 -
199 0.91 and 0.75 - 0.84, respectively. For replicate cores at the protein and corresponding transcript
200 levels the Spearman Rho were 0.38 - 0.51. In analyses of protein and transcript abundance in
201 correlations in other patient tumors, there were additionally 5,379 co-quantified proteins and
202 transcripts measured from LMD enriched tumor, stroma, and whole tumor from one level each
203 for cases 343WH and 343WB (Supplemental Table 17). Correlations were strongest within the
204 same LMD collection type (Supplemental Figure 2). For 343WH, the LMD enriched stroma
205 proteins correlated most strongly with the corresponding LMD enriched stroma transcripts, but
206 was also positively correlated with whole tumor transcripts, consistent with 343WM. The tumor
207 cellularity was marginally higher in 343WH (median tumor cellularity 85 - 95%) relative to
208 343WM (median tumor cellularity 80 - 95%) (Supplemental Table 1) which likely accounts for
209 differences in relatedness between the LMD enriched stroma protein and either whole tumor
210 RNA or LMD enriched stroma RNA,

211 We further used 281 antibodies (Supplemental Table 18) against native and/or post-
212 translationally modified proteins for RPPA analysis (Supplemental Table 19). Integrated
213 analyses of MS-based and RPPA proteome data (Supplemental Table 20) prioritized 54 proteins
214 as co-quantified between platforms and revealed similar findings as above indicating generally

215 positive correlation of protein abundances between LMD enriched tumor (Spearman Rho
216 between -0.24 and 0.59; Supplemental Fig. 5A) and stroma (Spearman Rho between 0.09 and
217 0.61; Supplemental Fig. 5B) across all cases, with the exceptions of LMD enriched tumor from
218 343VT and, to a lesser extent, 343WH showing mixed relatedness to other cases. However, the
219 whole tumor collections (Supplemental Fig. 5C) displayed markedly poorer concordance
220 (Spearman Rho between -0.50 and 0.49) between the two analytical platforms.

221 Comparison of proteomic and transcriptomic data revealed common canonical pathways
222 (Ingenuity Pathway Analysis, IPA) that were consistently altered within LMD collection types
223 (Supplemental Table 21). Aryl hydrocarbon receptor signaling, and the endocannabinoid cancer
224 inhibition pathway were among the top 5 canonical pathways most activated in LMD enriched
225 tumor epithelium relative to stroma at both the proteomic and transcriptomic level. Conversely,
226 IL-8 signaling and GP6 signaling were among the pathways predicted to be inhibited, i.e. least
227 activated in enriched tumor epithelium relative to stroma. Additional pathways differentially
228 expressed between tumor and stroma included activation of organismal death, morbidity and
229 mortality, bleeding, organization of the cytoplasm and skeleton, and cell movement and
230 migration in both proteome and transcriptome level data (Supplemental Table 22). Genes
231 encoding known drug targets of FDA-approved drugs [21] which were differentially expressed
232 (LIMMA adjusted p-value <0.01) between the LMD enriched tumor and LMD enriched stroma
233 were identified in the proteomic and transcriptomic data with Log_2 fold-changes > ±1 are listed
234 in Supplemental Table 23. The FDA-approved drugs targeting the identified genes include a
235 mixture of those being used currently for clinical management of HGSOC disease, such as
236 bevacizumab, as well as many drugs that are not. Similar results were not seen using the
237 proteomic data from case 343WM.

For the additional 9 HGSOC cases, we examined pathway enrichment using data for 381 proteins which displayed the same pattern of enrichment across all 9 cases, and which had Log_2 fold-changes > ±1 (Supplemental Table 24). Overall, the canonical pathways (Supplemental Tables 25, 26) enriched in LMD tumor epithelium relative to stroma generally overlapped with those from case 343WM suggesting these pathways are highly enriched within tumor or stroma cell populations of HGSOC tumors. The proteomic data from these 9 cases revealed protein targets of olaparib, estramustine, sorafenib, regorafenib, and pazopanib that were differentially expressed between LMD enriched tumor epithelium and stroma (Supplemental Table 27).

Intratumoral proteogenomic heterogeneity impacts prognostic molecular signatures correlating with altered disease outcome in HGSOC

Several large-scale studies have aimed to identify prognostic molecular signatures for HGSOC patient outcome, most of which have been from genomic and/or transcriptomic data from whole tumor specimen preparations from tumors that are typically qualified for inclusion using tumor cellularity/purity thresholds determined from pathologic inspection [3, 10, 22-26]. Per the categorization of tumors into immunoreactive, differentiated, proliferative, and mesenchymal subtypes, patients whose tumors are characterized by mesenchymal signatures have the worst prognosis. Consensus signatures generated by Chen *et al* [4] represent molecular subtype classifications and a random forest probability for composite classifiers generated from four historical HGSOC molecular subtypes classification systems [10, 22, 27, 28]. We used these consensus signatures to examine correlations between each spatially resolved tissue collection type to these HGSOC prognostic sub-types (Fig. 5; Supplemental Table 28; Supplemental Table 29). This analysis revealed that transcripts from LMD-enriched tumor cores and tumor

261 epithelium from case 343WM were strongly correlated with the differentiated and/or
262 proliferative subtypes and anti-correlated with the prognostically-poor mesenchymal subtype
263 (Fig. 5A). Conversely, transcripts from the LMD-enriched stroma most strongly correlated to the
264 prognostically-poor mesenchymal subtype. Molecular subtype profiles for enriched tumor and
265 stroma were largely recapitulated at the proteome level for case 343WM (Fig. 5A) and in the
266 additional 9 HGSOC cases (Fig. 5B). The whole tumor collections showed various levels of
267 correlation to all molecular subtypes, the extent to which seemingly depends on the percent
268 stromal and tumor epithelium admixture contributions to overall tumor purity.

269 We additionally investigated performance of a suboptimal cytoreduction associated
270 network (SCAN) signature [24] correlating with stroma activation and tumor invasiveness in
271 transcriptome data from case 343WM. The 11-gene surgical debulking signature from Liu *et al.*
272 most strongly correlated with our LMD-enriched stroma and whole tumor tissue collections,
273 (Supplemental Fig. 6), consistent with the correlation of the SCAN signature with stromal
274 involvement.

275 We next sought to explore molecular heterogeneity within each sample collection type
276 using a phylogenic analysis approach depicting relatedness between samples, which was
277 calculated based on similarities in protein abundance trends using Spearman correlations (Fig. 6;
278 Supplemental Table 30). In this way, the correlations of samples within the same LMD
279 collection type were calculated and then compared with those from another (as specified) LMD
280 collection type. Comparison of enriched tumor and stroma collections in case 343WM (Fig. 6A)
281 suggests that the proteome expression profiles of LMD enriched stroma are less heterogeneous
282 from a phylogenic perspective than either of the LMD enriched tumor epithelium collections,
283 and that the proteomic expression profile of whole tumor is more closely related to the LMD-

284 enriched stroma. Focusing only the LMD enriched tumor epithelium collections (cores and cross
285 sections) illustrates that (Fig. 6B) the degree of heterogeneity between all tumor cores is
286 significantly less than the degree of heterogeneity observed between LMD enriched tumor
287 collections ($p<0.0001$). Next, the correlations within and between the LMD enriched tumor
288 epithelium and stroma samples were calculated for cases 343WM, 343WK, 343WQ, and
289 343WH. These four cases were selected as they each have equal numbers of LMD enriched
290 tumor and stroma samples collected per case. In three of the four cases, the degree of
291 heterogeneity between tumor epithelium samples was significantly less ($p<0.01$) than the
292 heterogeneity observed in the stroma (Fig. 6C-F).

293 Striking examples of how regional tissue variations within a single tumor specimen can
294 impact molecular subtype classification and measurement of proteomic markers of interest are
295 highlighted for case 343WQ (Fig. 7), with similar findings seen across all cases (data not
296 shown). The relative composition of tumor epithelium and stroma are generally unchanged
297 throughout the depth of the specimen block (Fig. 7; left panel). The LMD enriched tumor and
298 stroma collections across each of the 5 levels displayed consistent patterns of molecular
299 abundances, correlations with HGSOC consensus molecular subtypes [4], and cellular admixture
300 scores [13], though the magnitude of the correlations varied by level (Fig. 7; right panel). In
301 contrast, the whole tumor collections displayed widely varied patterns of molecular abundances,
302 subtype classifications, and cellular admixture scores across the 5 levels.

303 Finally, we selected three patients in our expanded cohort for whom complete cancer-
304 related medical histories were available (Supplemental Figure 7) to analyze the heterogeneity of
305 clinical biomarker expression between LMD levels within each patients' specimen. Case 343WP
306 was extremely sensitive to chemotherapy and surviving with no evidence of disease as of last

follow-up, more than 5 years post-diagnosis. Cases 343WN and 343WQ had cancer-related deaths; these patients were moderately sensitive or refractory to chemotherapy, respectively. We generated a composite assessment of 70 genes or gene products analyzed in the clinical setting by Precision Therapeutics, Inc. (now Helomics (Pittsburgh, PA); a subsidiary of Predictive Oncology (Eagan, MN)), Caris Life Sciences (Irving, TX), Foundation Medicine (Cambridge, MA), Quest Diagnostics (Secaucus, NJ), and/or Ambry Genetics (Alisa Viejo, CA). Of these 70 markers, 31 were measured at the proteome level in our expanded cohort dataset. The variability of protein expression between levels for these markers was examined in cases 343WK, 343WQ, and 343WH, for whom the full complement of 5 levels/cases for all LMD collection types were available. Relative standard deviations (RSD) of protein expression were calculated and ranked to identify the top 5 most and least variable clinical markers (Supplemental Table 31). The most variable proteins between levels within a single patient's specimen in our whole tumor samples (comparable with the type of tissue examined in the clinic) were ABL1, NF1, MSH6, MLH1, and PTEN. None of these were among the top 5 most variable in our LMD enriched tumor samples. TOP1, RAD50, EPCAM, SMARCA4, and APC were the least variable in whole tumor. TUBB3 and HRAS were among the top 5 most variable proteins in both LMD enriched tumor and LMD enriched stroma, while FBN1 was among the least variable in both LMD enriched compartments.

Discussion

Ovarian cancers are typically diagnosed at an advanced stage after the accumulation of numerous molecular alterations [29]. In this study, we have demonstrated that LMD enrichment reveals extensive intratumoral proteogenomic heterogeneity, which has potential implications for

330 diagnostic, prognostic and therapeutic predictive value, and is similar to what has recently been
331 described in hepatocellular carcinoma [30].

332 In unsupervised hierarchical cluster analysis of proteins (Fig. 2A, 2C) and transcripts
333 (Fig. 2B, 2D), all LMD enriched cell populations exhibited similar protein and transcript
334 abundance trends. We found that many molecular alterations were negatively correlated with
335 established diagnostic and prognostic signatures within discrete cell populations, such as
336 confirmation of several mesenchymal marker genes as emerging from stroma cells in HGSOC
337 tissues recently identified by Zhang *et al.* [31] (Fig. 5). Furthermore, we observe a profoundly
338 unique transitioning of molecular subtype assignment based on sampling of the tumor
339 microenvironment at the level of the proteome versus the transcriptome (Fig. 5A). These
340 discrepancies are likely due to signature genes in molecular subtypes not being quantified in
341 proteome-level data or exhibiting lower correlation with transcript-level abundance. We further
342 note the correlation of protein and transcript abundance is higher in tumor epithelium versus
343 stroma collections and is likely attributed to the secretory nature of stroma cells [32]. This is
344 supported by the higher correlation of transcript abundance in stroma with protein abundance in
345 whole tumor collections for case 343WM (Fig. 4), though this also likely represents overall
346 tumor purity, as similar findings of higher correlation between stroma protein and whole tumor
347 transcripts were not seen in 343WH (Supplemental Fig. 4). This was further underscored by our
348 findings that the variance of proteins containing signal peptide sequences or classified as
349 "extracellular" by Gene Ontology across all levels from each LMD enriched tumor and stroma
350 was significantly greater ($p<0.0001$) than the variance of proteins lacking these classifications,
351 and the lack of differential MUC16 protein abundance between these tissue compartments
352 (Supplemental Fig. 3).

353 Comparison across proteomic platforms using proteins co-quantified by MS-based
354 proteomics and RPPA revealed similar findings as seen above with the co-quantified proteins
355 and transcripts in which there was general positive correlation within the same LMD enriched
356 tumor epithelium or stroma tissues across all cases (Supplemental Fig. 5A, B). However, there
357 was poor concordance between proteins measured in the whole tumor collections, often even
358 within the same case (Supplemental Fig. 5C). While this is likely partially attributable to the
359 limited number of features (54 proteins) used in this comparison [33], it largely recapitulates the
360 findings that whole tumor collections reflect overall levels of tumor purity and the need for cell
361 type enrichment for molecular characterization.

362 Our results suggest that molecular signatures developed to date have reflected variations
363 in tumor purity that differentially impact outcome; specifically, lower tumor purity contributes to
364 the assignment of tumors to poorer prognostic outcome (Fig. 5; Fig. 8). The predictive value for
365 estimating patient outcome through molecular subtype assignment (using the molecular
366 prognostic signatures identified by Konecny et al. [22]) showed a median survival difference of
367 two years depending on whether the tumor epithelium or stroma and/or mixed tissue is sampled.
368 Specifically, the mesenchymal subtype in the Konecny et al. study correlated with our LMD
369 enriched stroma and had a median overall survival (OS) of approximately 24 months whereas the
370 differentiated and proliferative subtypes correlated with our LMD enriched tumor and had a
371 median OS of approximately 48 months [22]. Notably, the contribution of the stromal
372 microenvironment to the mesenchymal signature has been recently described [31, 34, 35]. The
373 observation that poor prognosis molecular subtypes (namely, mesenchymal subtype) are driven
374 by the admixture of stroma cells supports the existence of a pathological ovarian stroma and
375 support the proposed role of cancer-associated fibroblasts contributing to disease development

376 and/or progression [36-39]. The presence of a large ovarian stromal compartment is an indicator
377 of poor prognosis [40]. Tumors with more interceding stroma have lower resectability,
378 decreasing the likelihood of achieving complete resection (R0) during surgical debulking leading
379 to worse outcome [41, 42]. Gene signatures in the ovarian stroma have also been correlated with
380 increased tumor invasiveness and metastatic spread to the blood and lymphatics [43]. However,
381 assignment of the cryopulverized tissue in our study to a particular subtype was less clear due to
382 profound signal averaging of the proteome (Fig. 5A). TCGA and other large-scale tumor
383 characterization efforts to date have applied pre-determined tumor purity cutoff levels to include
384 predominantly high purity tumors in their studies. As a result, molecular drivers of disease
385 progression specific to prognostically poor/low purity tumors are frequently missed [4, 44], as
386 recently realized for colon cancer [45] and gliomas [46].

387 We demonstrate the stromal distribution of many markers previously published as
388 correlative with residual disease and/or suboptimal cytoreduction in ovarian cancer
389 (Supplemental Fig. 6) [23, 24]. Among these, *FABP4* and *ADH1B* expression were associated
390 with significantly higher levels of residual disease [23]. Expression and shedding of AKAP12
391 has been recently described in isogenic cell line models of paclitaxel resistance and elevation of
392 AKAP12 transcript also correlated with decreased survival in HGSOC patients [47]. We observe
393 AKAP12 transcript is elevated in stroma versus tumor epithelium (Supplemental Tables 5, 6, 7,
394 8) suggesting that elevation of AKAP12 in drug-resistant HGSOC cells may be due to
395 chemotherapy-induced epithelial to mesenchymal transition and association with poor disease
396 outcome may correlate with patients harboring lower-purity, likely mesenchymal-subtype
397 tumors. *COL11A1* transcripts were also abundant in the stroma and some of the whole tumor

collections (Supplemental Fig. 6), consistent with findings that COL11A1 is elevated in cancer-associated fibroblasts (CAFs) [37].

Extensive intratumor heterogeneity was observed in our study within each of the LMD enriched tumor and stroma compartments, as demonstrated by the tumor cores from case 343WM and between the spatially separated collection levels for each of the 10 HGSOC cases assessed. A comparison of the magnitude of heterogeneity within each LMD enriched tissue type revealed that overall there was a greater amount of heterogeneity in the stroma tissue relative to tumor epithelium (Fig. 6C-F). Though more related than the stroma collections, we demonstrate heterogeneity within the tumor epithelium resulting from locoregional differences, as replicate tumor cores displayed greater relatedness to each other than to LMD enriched tumor collections taken from the entire tissue area (Fig. 6A, B). Consistent with our enriched tumor and stroma cell findings, single cell RNA sequencing on HGSOC has previously revealed that individual cells of the same tissue type (tumor epithelium or stroma) differentially clustered with molecular subtypes due to unique gene expression profiles [48]. Further, heterogeneity within HGSOC molecular subtypes has been partially attributed to activation of distinct transcriptional factors serving as master regulators of the cellular phenotypes [49]. As mentioned, within the ovarian stromal microenvironment we observed the highest probability of classification as mesenchymal and/or immunoreactive subtypes (Fig. 5).

Compartmentalized expression of genes encoding known FDA-approved anticancer drug targets [21] was found in both the LMD enriched tumor epithelium and stroma collections (Supplemental Tables 23, 27). The proteins encoded by *VEGFA* and *FLT1* (also known as *VEGFR1*) are targets of bevacizumab, a monoclonal antibody often used as an anti-angiogenic therapy for treating HGSOC patients [50]. In our study, *VEGFA* transcript expression from case

421 343WM was significantly enriched in tumor epithelium whereas transcript expression of
422 *FLT1*/*VEGFR1* was more abundant in LMD enriched stroma (Supplemental Table 23).
423 Dysregulated VEGF/VEGFR expression has been demonstrated to contribute to epithelial
424 ovarian cancer development and/or progression through increased vascularization and improved
425 survival of endothelial cells via anti-apoptotic signaling in the newly formed vessels [51, 52],
426 though bevacizumab targeting of VEGF/VEGFR has disputed levels of improvement on HGSOC
427 patient survival [53]. PARP1 protein was consistently enriched in the tumor epithelium of 9
428 patients in our study (Supplemental Table 27). Olaparib, rucaparib, and niraparib are poly(ADP-
429 ribose) polymerase (PARP) inhibitors used for treating HGSOC patients in either the recurrent or
430 maintenance setting [54]. Conversely, MAP1A is a target of estramustine and PDGFRB is a
431 target of sorafenib, regorafenib, and pazopanib; MAP1A and PDGFRB proteins were both found
432 to be significantly enriched in LMD stroma.

433 Accurate diagnosis and estimation of prognostic outcome are of utmost interest to
434 patients, so we analyzed the intratumor heterogeneity of protein expression for gene and/or
435 protein markers that are routinely assessed in HGSOC patients. Specifically, we examined the
436 variability of protein expression between each of the 5 levels per LMD collection type separately
437 for cases 343WK, 343WQ, and 343WH and reported proteins that were most and least variable
438 within each LMD collection type (Supplemental Table 31). Our whole tumor samples represent
439 the types of samples analyzed in the clinical setting. ABL1 was among the top 5 most variable
440 proteins in whole tumor samples within each patient's tumor. ABL1 is a target of the drug
441 Regorafenib which is currently FDA-approved for treatment of colorectal and stomach cancers
442 [55] and has been the subject of recent clinical trials for treatment of recurrent epithelial ovarian
443 cancers. Interim clinical trial results reported Regorafenib to be inefficacious in improving

444 progression free survival, overall survival, or overall response rate. Our results suggest that the
445 clinical inefficacy of Regorafenib for treating ovarian cancers could, at least in part, be attributed
446 to the high intratumoral heterogeneity of expression of ABL1 or other related proteins. MSH6
447 and MLH1 were also among the top 5 most variable proteins in this analysis. MSH6 and MLH1
448 are biomarkers of mismatch repair and microsatellite instability and are used as prognostic
449 indicators of improved survival and clinical response to platinum-based chemotherapy [56]. The
450 high levels of intratumoral heterogeneity of MSH6 and MLH1 in our study suggest that the
451 predictive efficacy of platinum-based chemotherapies may not adequately represent true patient
452 response due to the potential for sampling variations of regional protein expression within a
453 tumor biopsy. TUBB3 is the target of the drug Ixabepilone, FDA-approved for treatment of
454 breast cancer [55] and the subject of recent clinical trials for potential use in patients with
455 recurrent or persistent platinum- and taxane-resistant ovarian cancer [57], which showed
456 promising results. Surprisingly, TUBB3 was among the top 5 most variable proteins in both
457 LMD enriched tumor and LMD enriched stroma in our analysis.

458 In conclusion, we demonstrate a critical need to account for cellular subtype and regional
459 TME proteogenomic heterogeneity in cancer molecular profiling efforts that will substantially
460 enable in-depth characterization of spatially distributed subclonal cell populations that have
461 underappreciated roles in driving carcinogenesis. Further work to deconstruct the TME will aid
462 clinical diagnosis, improve the efficacy of therapeutic intervention, and increase capabilities to
463 identify druggable molecular markers of disease development and progression.

464

Materials and Methods

Tissue specimens

Surgically resected fresh-frozen tumor tissue specimens were obtained from ten patients with HGSOC of primary ovarian or tubo-ovarian origin. These comprised a mixture of chemotherapy-naïve specimens and specimens obtained following neoadjuvant chemotherapy (NACT) from patients with advanced stage (stage III or IV) disease. The specific tissues used for the study were from ovary, omentum, and pelvic or adnexa masses. The tissue blocks were sectioned by cryotome into 170 - 210 consecutive 10 μm thin tissue sections (1.7 - 2.1 mm total depth) which were placed on PEN membrane slides (Leica Microsystems). Representative sections were mounted on charged glass slides and stained with hematoxylin and eosin (H&E) after every 10 PEN membrane slide sections (100 μm), except for case 343WM where representative H&E slides were generated after every 20 PEN membrane slide sections (200 μm).

Laser microdissection

The specimen obtained from case 343WM was uniquely prepared for laser microdissection (LMD) and proteogenomic analysis of spatially separated tumor "cores" which represent defined sub-populations of tumor epithelium that were collected as technical replicate areas for comparison with tumor epithelium collected from larger whole slide areas. Four regionally separated areas within the tissue were laser microdissected to enrich tumor epithelium (LMD7, Leica Microsystems) from each of 100 slides for proteomics or 50 slides for transcriptomics. The cores were pooled from a cross-sectional area of approximately 1 mm^2 collected by LMD per slide for a depth spanning the entire block (1 mm x 1 mm x 2 mm). An

488 adjacent 1 mm^2 was microdissected to serve as a replicate from each core; in total each core plus
489 their respective adjacent replicate regions covered an approximate 2 mm^3 aggregate volume of
490 tumor epithelium. The distance between the center of each tumor core and the center of the
491 nearest neighboring core was approximately 4 mm. For a set of 9 sections (200 µm apart) each
492 for proteomics and transcriptomics, all remaining tumor epithelium (between 20 - 44
493 mm^2/section) and stroma (44 - 80 mm^2/section) were collected by LMD after the core regions
494 were collected. Whole tumor tissue was collected from a second set of 9 sections (96 - 155
495 mm^2/section), where only regions containing necrosis, blood, and fat were excluded.

496 For the remaining 9 HGSOC cases, the slides from each block were separated into five
497 equal levels (quintiles) assigned by depth within the block. Slides designated for MS proteomics
498 (n=9 patients, 5 levels each), reverse phase protein array (RPPA; n=8 patients, 5 levels each, plus
499 8 levels from 343WM), and transcriptomics (n=2 patients, 1 level each) within each level were
500 interlaced as much as possible.

501 All slides were H&E stained prior to LMD. For the slides microdissected for mass
502 spectrometry (MS) proteomics, phosphatase inhibitors (Sigma Aldrich) were added to the 70%
503 ethanol fixative and the first DEPC water; slides for transcriptomics were stained with RNase
504 inhibitors (ProtectRNA; Sigma Aldrich) added into all aqueous solutions. Slide preparation for
505 RPPA did not involve staining with eosin after the hematoxylin but included color development
506 in Scott's Tap Water (Thermo Fisher Scientific) and two final drying steps in xylenes. Protease
507 inhibitors (Roche) were added to all RPPA staining solutions except for the 100% ethanol and
508 xylene washes.

509 Within each quintile level per specimen block LMD was used to enrich cross-sectional
510 areas of 40 mm^2 and 15 mm^2 (LMD enriched tumor epithelium, LMD enriched stroma, and

whole tumor) for analysis via liquid chromatography-tandem mass spectrometry (LC-MS/MS) and reverse phase protein microarray (RPPA), respectively. For two cases (343WH and 343WB), a cross-sectional area of 25 mm^2 of each LMD enriched tumor, LMD enriched stroma, and whole tumoe was collected from one level for RNA sequencing (RNA-seq). Microdissected tissue was collected into LC-grade water (Fisher Scientific), a tissue extraction/lysis buffer, or Buffer RLT (Qiagen) for analysis via LC-MS/MS, RPPA, and RNA-seq, respectively. The RPPA extraction/lysis buffer consisted of a 1:1 mixture of Tissue Protein Extraction Reagent (T-PER; Pierce), Novex 2x Tris-Glycine SDS Sample Buffer (Invitrogen), plus 2.5% *v*/*v* 2-mercaptoethanol which was added to tissue at a ratio of 3 µl buffer per 1 mm^2 LMD tissue. For RPPA, each slide spent no more than 30 min dwell time on the LMD microscope. Additional slides were collected into new tubes. Collected tissue was briefly centrifuged and frozen at -80 °C until analysis.

OracleBio image analysis

Pre- and post-LMD images were collected using the Aperio ScanScope XT slide scanner (Leica Microsystems). Image analysis was performed by OracleBio using the Indica Labs HALO platform. Post-LMD images from 343WM were used to develop classification algorithms for identification of the "dissection area" and "all remaining tissue". A separate algorithm was developed which involved co-registration of post-LMD images with corresponding adjacent H&E-stained sections on glass slides for detection and quantification of the cell nuclei abundance within the LMD regions. The size and number of cells and nuclei collected in each LMD collection was determined using matched sets of reference glass H&E sections and PEN membrane slides following LMD enrichment of tumor (n=15) and stroma (n=6) cell populations.

534

535 ***Peptide preparation for TMT LC-MS/MS***

536 LMD tissue in LC-grade water was dried, re-suspended in 100 mM triethylammonium
537 bicarbonate (TEAB)/10% acetonitrile (ACN), and digested using SMART trypsin (1 µg/30 mm^2
538 tissue; Thermo Fisher) and pressure cycling technology (PCT, Pressure Biosciences, Inc.) [58].
539 For 343WM, the remaining tissue in the OCT block was washed with water and cryopulverized
540 in liquid nitrogen in a mortar and pestle. The cryopulverized tissue was re-suspended in 100 mM
541 TEAB/10% ACN and digested by PCT using SMART trypsin (1 µg protease/ 30 mm^2 tissue).
542 Peptide concentrations from trypsin digests were determined using the bicinchoninic acid assay
543 (Pierce BCA). Tryptic peptides were labeled with isobaric Tandem Mass Tags (TMT) according
544 to the manufacturer's instructions using the TMT 10-Plex Kit or TMTpro 16-Plex Kit from
545 Thermo Fisher (Supplemental Table 4). The TMT 10-Plex reagents and TMTpro 16-plex
546 reagents were used for labeling samples from case 343WM the remaining nine cases,
547 respectively, to generate patient-specific TMT plexes. Briefly, peptide samples were individually
548 mixed with respective TMT reagents for 1 h at room temperature, then quenched using 5%
549 hydroxylamine. Empty TMT channels were filled using equal amounts of peptide mixed from
550 each of the 5 levels of the whole tumor collections in the respective patient-specific plex.

551 Each TMT-10 or TMTpro-16 multiplex set of samples were loaded onto a C-18 trap
552 column in 10 mM NH_4HCO_3 (pH 8.0) and fractionated by basic reversed-phase liquid
553 chromatography (bRPLC) into 96 fractions through development of a linear gradient of
554 acetonitrile (0.69% acetonitrile/min). For 343WM, 36 concentrated fractions were generated by
555 pooling in a serpentine manner, each of which were analyzed for LC-MS/MS. For the remaining

9 cases, 24 concentrated fractions were generated following bRPLC which were individually analyzed by LC-MS/MS.

Liquid chromatography-tandem mass spectrometry

The TMT-10 or TMTpro-16 sample multiplex bRPLC fractions were analyzed by LC-MS/MS employing a nanoflow LC system (EASY-nLC 1200, ThermoFisher Scientific, Inc.) coupled online with an Orbitrap Fusion Lumos Tribrid MS (ThermoFisher Scientific, Inc.). In brief, each sample was loaded on a nanoflow HPLC system outfitted with a reversed-phase trap column (Acclaim PepMap100 C18, 2 cm, nanoViper, ThermoFisher Scientific, Inc) and a heated (50 °C) reversed-phase analytical column (Acclaim PepMap RSLC C18, 2 µm, 100 Å, 75 µm × 500 mm, nanoViper, ThermoFisher Scientific, Inc) connected online with an Orbitrap mass spectrometer. Peptides were eluted by developing a linear gradient of 2% mobile phase B (95% acetonitrile with 0.1% formic acid) to 32% mobile phase B within 120 min at a constant flow rate of 250 nL/min. High resolution (R=60,000 at *m/z* 200) broadband (*m/z* 400 – 1,600) mass spectra (MS) were acquired from which the top 12 most intense molecular ions in each MS scan were selected for high-energy collisional dissociation (HCD, normalized collision energy of 38%) acquisition in the orbitrap at high resolution (R=50,000 at *m/z* 200). Monoisotopic precursor selection mode was set to "Peptide" and MS1 peptide molecular ions selected for HCD were restricted to z = +2, +3 and +4. The RF lens was set to 30% and both MS1 and MS2 spectra were collected in profile mode. Dynamic exclusion (t=20s at a mass tolerance=10 ppm) was enabled to minimize redundant selection of peptide molecular ions for HCD.

Quantitative proteomic data processing pipeline for global proteome analysis

579 Peptide identifications were generated by searching the .raw data files with a publicly-
580 available, non-redundant human proteome database (Swiss-Prot, Homo sapiens, Proteome
581 UP000005640, 20,257 sequences, downloaded 12-01-2017; http://www.uniprot.org/) appended
582 with porcine trypsin (Uniprot: P00761) sequences using Mascot (Matrix Science) and Proteome
583 Discoverer (Thermo Fisher Scientific). Identification, normalization, and Log_2 transformation of
584 PSMs was performed as previously described [58] for calculation of protein-level abundances.
585
586 ***RNA sequencing***
587 Tissue collected by LMD in Buffer RLT was purified using the RNeasy Micro Kit
588 (Qiagen) per the manufacturer's instructions. RNA concentrations were determined by
589 fluorescence (Qubit HS and BR kits, Thermo Fisher). RNA integrity numbers (RIN) were
590 calculated using the RNA 6000 Pico Kit 2100 Bioanalyzer (Agilent). All RNA was high-quality
591 with RIN values of 7.2 or greater, except for two samples which had RIN values of 4.9 and 6.5.
592 RNA samples were reverse transcribed from 10 ng input using the SuperScript VILO
593 cDNA Synthesis Kit. Barcoded cDNA libraries containing 5-6 LMD samples plus a Universal
594 Human Reference RNA (UHR) standard (Stratagene) were prepared on the Ion Chef System
595 using the Ion Ampliseq Chef DL8 materials and the Ion AmpliSeq Transcriptome Human Gene
596 Expression Panel Chef-ready Kit (Thermo Fisher). Libraries were then purified via solid phase
597 reversible immobilization (SPRI) using AMPure XP beads (Beckman Coulter) to remove
598 fragments less than 100 bp, quantified by qPCR (TaqMan Quantitation Kit; Applied
599 Biosystems), and 25 µl of 100 pM diluted library was used for templating, amplification via
600 emulsion PCR, and loaded onto Ion 550 chips on the Ion Chef System.
601 Sequencing was performed on the Ion Torrent S5 XL (Thermo Fisher) and mapped to the
602 hg19 human reference transcriptome (hg19_Ampliseq_Transcriptome_21K_v1). Successful

603 sequencing runs achieved ≥18M reads/sample (with one exception) and 169-234X AQ20 mean
604 coverage depth. Per the Torrent Suite Software (Torrent Suite v5.8.0), the number of reads
605 aligning to a given gene target represents an expression value referred to as "counts". The read
606 count per million mapped reads (RPM) for each barcoded sample was calculated by the software
607 as read count x 10^6 / total number of mapped reads. Normalized RPM-level transcript
608 abundances were calculated relative to the average RPM abundance quantified across all samples
609 for a given transcript and Log_2 transformed.
610

611 ***Bioinformatic and statistical analyses***

612 Unsupervised analyses were performed using proteins or transcripts exhibiting a median
613 absolute deviation (MAD) >0.5 across all samples and clustered by Pearson correlation as
614 heatmaps using Clustvis (version 1.2.0) in R (version 3.6.2). Differential analyses of global
615 proteome and transcript data matrixes was performed using LIMMA (version 3.8, [59]) in R
616 (version 3.6.2); features satisfying a LIMMA p-value <0.01 and exhibiting a Log_2 fold-change
617 cut-off ±1 were prioritized for downstream analyses. Cell type enrichment analyses were
618 performed using RPM-level RNA-seq data in xCell (http://xcell.ucsf.edu/; version 1.1.0 [60]).
619 xCell cell type signature scores of interest were categorized by relative rank from highest to
620 lowest spanning a range of 1 to -1 to enable co-visualization with similarly categorized transcript
621 and protein abundance for candidates of interest. Boxplots of relative protein abundances or cell
622 type signature scores were generated using Ggplot2 (version 3.2.1). Random forest probabilities
623 for classification of consensus molecular subtypes using either global proteome or transcriptome
624 data were calculated using consensusOV (version 1.8.1). Dendrograms were generated using
625 Ggtree (version 2.0.1) using features with MAD>1 across individual patient samples, with the

exception of the comparison between tumor cores and LMD enriched tumor from case 343WM, which used features with MAD>0.5. Tree structure was determined by neighbor-joining tree estimation using Ape (version 5.3) and Spearman correlations between samples were calculated. Molecular subtype classifications were compared by Spearman correlation using MedCalc (version 19.0.7). Functional pathway inference and drug targets were assessed using Ingenuity Pathway Analysis. The heatmap in Fig. 7 was generated using ComplexHeatmap (version 2.2.0); the heatmaps in Supplementary Fig. 4 and 5 were generated using Morpheus (https://software.broadinstitute.org/morpheus/; version 1.0-1).

Reverse phase protein microarray

Using an Aushon 2470 arrayer (Aushon BioSystems, Billerica, MA) equipped with 185 μm pins, cell lysates along with internal reference standards were immobilized onto nitrocellulose-coated slides (Grace Bio-labs, Bend, OR) in technical replicates (n=3). To assess the amount of protein in each sample and for normalization purposes, selected arrays were stained with Sypro Ruby Protein Blot Stain (Molecular Probes, Eugene, OR) following manufacturer's instructions. Immunostaining was performed as previously described [61, 62]. In brief, prior to antibody staining, arrays were first treated with Reblot Antibody Stripping solution (Chemicon, Temecula, CA) for 15 minutes at room temperature, washed with PBS and incubated I-block (Tropix, Bedford, MA). To reduce unspecific binding between endogenous proteins and the detection system, arrays were then probed with 3% hydrogen peroxide, an avidin/biotin blocking system (Dako Cytomation, Carpinteria, CA), and an additional serum free protein block (Dako Cytomation, Carpinteria, CA) using an automated system (Dako Cytomation, Carpinteria, CA). Each array was then probed with one polyclonal or monoclonal primary antibody targeting

649 a protein of interest. Primary antibodies' specificity was previously assessed on commercial cell
650 lysates or human tissue lysates by western blotting [63]. The criteria for validation were the
651 presence of a single band of correct molecular weight in the positive control sample and the
652 absence of a band in the negative control. Antibodies targeting phosphorylated epitopes were
653 additionally validated by ligand induction. A subset of antibodies was further validated against
654 peptide competition. Arrays were probed with total of 281 antibodies targeting native and/or
655 post-translationally modified proteins. Primary antibodies were recognized by a biotinylated
656 anti-rabbit (Vector Laboratories, Inc.) or anti-mouse secondary antibody (Dako Cytomation,
657 Carpinteria, CA). Signal amplification was achieved using a commercially available tyramide-
658 based avidin/biotin amplification system (Dako Cytomation, Carpinteria, CA) coupled with
659 fluorescent detection using the streptavidin-conjugated IRDye680 dye (LI-COR Biosciences,
660 Lincoln, NE), according to the manufacturer's instructions. Selected arrays were incubated with
661 the secondary antibodies alone to capture background and unspecific signal. Images were
662 acquired using a laser scanner (TECAN PowerScanner, Mönnedorf, Switzerland) and analyzed
663 using a commercially available software (MicroVigene V5.1.0.0; Vigenetech, Carlisle, MA). In
664 brief, the software performed spot finding and subtraction of the local background/unspecific
665 signal. Finally, each sample was normalized to the corresponding amount of protein derived
666 from the Sypro Ruby stained slides and triplicates were averaged.
667
668

References

1. Siegel, R.L., K.D. Miller, and A. Jemal, *Cancer statistics, 2020.* CA: A Cancer Journal for Clinicians, 2020. **70**(1): p. 7-30.
2. Noone AM, H.N., Krapcho M, Miller D, Brest A, Yu M, Ruhl J, Tatalovich Z, Mariotto A, Lewis DR, Chen HS, Feuer EJ, Cronin KA (eds), *SEER Cancer Statistics Review, 1975-2015.* National Cancer Institute. Bethesda, MD, https://seer.cancer.gov/csr/1975_2015/, April 2018. **based on November 2017 SEER data submission, posted to the SEER web site**.
3. The Cancer Genome Atlas Research, N., *Integrated genomic analyses of ovarian carcinoma.* Nature, 2011. **474**: p. 609.
4. Chen, G.M., et al., *Consensus on Molecular Subtypes of High-Grade Serous Ovarian Carcinoma.* Clinical Cancer Research, 2018. **24**(20): p. 5037-5047.
5. Jimenez-Sanchez, A., et al., *Heterogeneous Tumor-Immune Microenvironments among Differentially Growing Metastases in an Ovarian Cancer Patient.* Cell, 2017. **170**(5): p. 927-938 e20.
6. Schwarz, R.F., et al., *Spatial and Temporal Heterogeneity in High-Grade Serous Ovarian Cancer: A Phylogenetic Analysis.* PLOS Medicine, 2015. **12**(2): p. e1001789.
7. Shih, A.J., et al., *Identification of grade and origin specific cell populations in serous epithelial ovarian cancer by single cell RNA-seq.* PloS one, 2018. **13**(11): p. e0206785-e0206785.
8. Zhang, A.W., et al., *Interfaces of Malignant and Immunologic Clonal Dynamics in Ovarian Cancer.* Cell, 2018. **173**(7): p. 1755-1769.e22.
9. Bashashati, A., et al., *Distinct evolutionary trajectories of primary high-grade serous ovarian cancers revealed through spatial mutational profiling.* The Journal of Pathology, 2013. **231**(1): p. 21-34.
10. Verhaak, R.G.W., et al., *Prognostically relevant gene signatures of high-grade serous ovarian carcinoma.* The Journal of clinical investigation, 2013. **123**(1): p. 517-525.
11. Yang, X., et al., *FAP Promotes Immunosuppression by Cancer-Associated Fibroblasts in the Tumor Microenvironment via STAT3–CCL2 Signaling.* Cancer Research, 2016. **76**(14): p. 4124-4135.
12. Ghosh, S., et al., *Up-regulation of stromal versican expression in advanced stage serous ovarian cancer.* Gynecologic oncology, 2010. **119**(1): p. 114-120.
13. Aran, D., Z. Hu, and A.J. Butte, *xCell: digitally portraying the tissue cellular heterogeneity landscape.* Genome biology, 2017. **18**(1): p. 220-220.
14. Vergote, I.B., O.P. Børmer, and V.M. Abeler, *Evaluation of serum CA 125 levels in the monitoring of ovarian cancer.* American Journal of Obstetrics & Gynecology, 1987. **157**(1): p. 88-92.
15. Bast, R.C., et al., *A Radioimmunoassay Using a Monoclonal Antibody to Monitor the Course of Epithelial Ovarian Cancer.* New England Journal of Medicine, 1983. **309**(15): p. 883-887.
16. Canney, P.A., et al., *Ovarian cancer antigen CA125: a prospective clinical assessment of its role as a tumour marker.* British Journal of Cancer, 1984. **50**(6): p. 765-769.
17. Yin, B.W.T., A. Dnistrian, and K.O. Lloyd, *Ovarian cancer antigen CA125 is encoded by the MUC16 mucin gene.* International Journal of Cancer, 2002. **98**(5): p. 737-740.
18. O'Brien, T.J., et al., *The CA 125 Gene: An Extracellular Superstructure Dominated by Repeat Sequences.* Tumor Biology, 2001. **22**(6): p. 348-366.
19. O'Brien, T.J., et al., *The CA 125 Gene: A Newly Discovered Extension of the Glycosylated N-Terminal Domain Doubles the Size of This Extracellular Superstructure.* Tumor Biology, 2002. **23**(3): p. 154-169.
20. Fendrick, J.L., et al., *Characterization of CA 125 Synthesized by the Human Epithelial Amnion WISH Cell Line.* Tumor Biology, 1993. **14**(5): p. 310-318.

715 21. Sun, J., et al., *A systematic analysis of FDA-approved anticancer drugs.* BMC systems biology,
716 2017. **11**(Suppl 5): p. 87-87.
717 22. Konecny, G.E., et al., *Prognostic and therapeutic relevance of molecular subtypes in high-grade*
718 *serous ovarian cancer.* Journal of the National Cancer Institute, 2014. **106**(10): p. dju249.
719 23. Tucker, S.L., et al., *Molecular biomarkers of residual disease after surgical debulking of high-*
720 *grade serous ovarian cancer.* Clinical cancer research : an official journal of the American
721 Association for Cancer Research, 2014. **20**(12): p. 3280-3288.
722 24. Liu, Z., et al., *Suboptimal cytoreduction in ovarian carcinoma is associated with molecular*
723 *pathways characteristic of increased stromal activation.* Gynecologic oncology, 2015. **139**(3): p.
724 394-400.
725 25. Leong, H.S., et al., *Efficient molecular subtype classification of high-grade serous ovarian cancer.*
726 The Journal of Pathology, 2015. **236**(3): p. 272-277.
727 26. Wang, C., et al., *Pooled Clustering of High-Grade Serous Ovarian Cancer Gene Expression Leads*
728 *to Novel Consensus Subtypes Associated with Survival and Surgical Outcomes.* Clinical cancer
729 research : an official journal of the American Association for Cancer Research, 2017. **23**(15): p.
730 4077-4085.
731 27. Helland, Å., et al., *Deregulation of MYCN, LIN28B and LET7 in a molecular subtype of aggressive*
732 *high-grade serous ovarian cancers.* PloS one, 2011. **6**(4): p. e18064-e18064.
733 28. Bentink, S., et al., *Angiogenic mRNA and microRNA Gene Expression Signature Predicts a Novel*
734 *Subtype of Serous Ovarian Cancer.* PLOS ONE, 2012. **7**(2): p. e30269.
735 29. Torre, L.A., et al., *Ovarian cancer statistics, 2018.* CA: A Cancer Journal for Clinicians, 2018. **68**(4):
736 p. 284-296.
737 30. Buczak, K., et al., *Spatial Tissue Proteomics Quantifies Inter- and Intratumor Heterogeneity in*
738 *Hepatocellular Carcinoma (HCC).* Molecular & Cellular Proteomics, 2018. **17**(4): p. 810-825.
739 31. Zhang, Q., C. Wang, and W.A. Cliby, *Cancer-associated stroma significantly contributes to the*
740 *mesenchymal subtype signature of serous ovarian cancer.* Gynecologic Oncology, 2019. **152**(2):
741 p. 368-374.
742 32. Furuya, M., *Ovarian cancer stroma: pathophysiology and the roles in cancer development.*
743 Cancers, 2012. **4**(3): p. 701-724.
744 33. Ali, M., et al., *Global proteomics profiling improves drug sensitivity prediction: results from a*
745 *multi-omics, pan-cancer modeling approach.* Bioinformatics, 2017. **34**(8): p. 1353-1362.
746 34. Izar, B., et al., *A single-cell landscape of high-grade serous ovarian cancer.* Nature Medicine,
747 2020.
748 35. Schwede, M., et al., *The Impact of Stroma Admixture on Molecular Subtypes and Prognostic*
749 *Gene Signatures in Serous Ovarian Cancer.* Cancer Epidemiol Biomarkers Prev, 2020. **29**(2): p.
750 509-519.
751 36. Bu, L., et al., *Biological heterogeneity and versatility of cancer-associated fibroblasts in the tumor*
752 *microenvironment.* Oncogene, 2019.
753 37. Jia, D., et al., *A COL11A1-correlated pan-cancer gene signature of activated fibroblasts for the*
754 *prioritization of therapeutic targets.* Cancer letters, 2016. **382**(2): p. 203-214.
755 38. Narikiyo, M., et al., *Molecular association of functioning stroma with carcinoma cells in the*
756 *ovary: A preliminary study.* Oncology letters, 2019. **17**(3): p. 3562-3568.
757 39. Eckert, M.A., et al., *Proteomics reveals NNMT as a master metabolic regulator of cancer-*
758 *associated fibroblasts.* Nature, 2019.
759 40. Labiche, A., et al., *Stromal Compartment as a Survival Prognostic Factor in Advanced Ovarian*
760 *Carcinoma.* International Journal of Gynecologic Cancer, 2010. **20**(1): p. 28-33-28-33.

41. Torres, D., et al., *Factors that influence survival in high-grade serous ovarian cancer: A complex relationship between molecular subtype, disease dissemination, and operability.* Gynecologic Oncology, 2018. **150**(2): p. 227-232.
42. Hamilton, C.A., et al., *The impact of disease distribution on survival in patients with stage III epithelial ovarian cancer cytoreduced to microscopic residual: a Gynecologic Oncology Group study.* Gynecologic oncology, 2011. **122**(3): p. 521-526.
43. Yue, H., et al., *Gene signature characteristic of elevated stromal infiltration and activation is associated with increased risk of hematogenous and lymphatic metastasis in serous ovarian cancer.* BMC Cancer, 2019. **19**(1): p. 1266.
44. Aran, D., M. Sirota, and A.J. Butte, *Systematic pan-cancer analysis of tumour purity.* Nature Communications, 2015. **6**: p. 8971.
45. Mao, Y., et al., *Low tumor purity is associated with poor prognosis, heavy mutation burden, and intense immune phenotype in colon cancer.* Cancer management and research, 2018. **10**: p. 3569-3577.
46. Zhang, C., et al., *Tumor Purity as an Underlying Key Factor in Glioma.* Clinical Cancer Research, 2017. **23**(20): p. 6279-6291.
47. Bateman, N.W., et al., *Elevated AKAP12 in paclitaxel-resistant serous ovarian cancer cells is prognostic and predictive of poor survival in patients.* Journal of proteome research, 2015. **14**(4): p. 1900-1910.
48. Winterhoff, B.J., et al., *Single cell sequencing reveals heterogeneity within ovarian cancer epithelium and cancer associated stromal cells.* Gynecologic oncology, 2017. **144**(3): p. 598-606.
49. Zhang, S., et al., *Stroma-associated master regulators of molecular subtypes predict patient prognosis in ovarian cancer.* Scientific reports, 2015. **5**: p. 16066-16066.
50. Rossi, L., et al., *Bevacizumab in ovarian cancer: A critical review of phase III studies.* Oncotarget, 2017. **8**(7): p. 12389-12405.
51. Skirnisdottir, I., T. Seidal, and H. Åkerud, *The relationship of the angiogenesis regulators VEGF-A, VEGF-R1 and VEGF-R2 to p53 status and prognostic factors in epithelial ovarian carcinoma in FIGO-stages I-II.* International journal of oncology, 2016. **48**(3): p. 998-1006.
52. Masoumi Moghaddam, S., et al., *Significance of vascular endothelial growth factor in growth and peritoneal dissemination of ovarian cancer.* Cancer metastasis reviews, 2012. **31**(1-2): p. 143-162.
53. Tewari, K.S., et al., *Final Overall Survival of a Randomized Trial of Bevacizumab for Primary Treatment of Ovarian Cancer.* Journal of Clinical Oncology. **0**(0): p. JCO.19.01009.
54. Jiang, X., et al., *PARP inhibitors in ovarian cancer: Sensitivity prediction and resistance mechanisms.* Journal of cellular and molecular medicine, 2019. **23**(4): p. 2303-2313.
55. Sun, J., et al., *A systematic analysis of FDA-approved anticancer drugs.* BMC Syst Biol, 2017. **11**(Suppl 5): p. 87.
56. Zhao, C., et al., *Prognostic values of DNA mismatch repair genes in ovarian cancer patients treated with platinum-based chemotherapy.* Arch Gynecol Obstet, 2018. **297**(1): p. 153-159.
57. De Geest, K., et al., *Phase II clinical trial of ixabepilone in patients with recurrent or persistent platinum- and taxane-resistant ovarian or primary peritoneal cancer: a gynecologic oncology group study.* J Clin Oncol, 2010. **28**(1): p. 149-53.
58. Lee, S., et al., *Molecular Analysis of Clinically Defined Subsets of High-Grade Serous Ovarian Cancer.* Cell Rep, 2020. **31**(2): p. 107502.
59. Ritchie, M.E., et al., *limma powers differential expression analyses for RNA-sequencing and microarray studies.* Nucleic Acids Research, 2015. **43**(7): p. e47-e47.
60. Aran, D., Z. Hu, and A.J. Butte, *xCell: digitally portraying the tissue cellular heterogeneity landscape.* Genome Biol, 2017. **18**(1): p. 220.

809 61. Baldelli, E., et al., *Reverse Phase Protein Microarrays*, in *Molecular Profiling: Methods and*
810 *Protocols*, V. Espina, Editor. 2017, Springer New York: New York, NY. p. 149-169.
811 62. Baldelli, E., et al., *Functional signaling pathway analysis of lung adenocarcinomas identifies*
812 *novel therapeutic targets for KRAS mutant tumors.* Oncotarget, 2015. **6**(32): p. 32368-32379.
813 63. Signore, M. and K.A. Reeder, *Antibody validation by Western blotting.* Methods Mol Biol, 2012.
814 **823**: p. 139-55.

815

816

Acknowledgements: This study was supported in part by the U.S. Department of Defense - Uniformed Services University of the Health Sciences (HU0001-16-2-0006 and HU0001-16-2-0014) and the Ovarian Cancer Research Program from the Congressionally Directed Medical Research Program (W81XWH-16-2-0038). The authors would like to acknowledge Lorcan Sherry and Mark Anderson from OracleBio Limited (Scotland, UK) for histopathology image analysis support. The authors would like to acknowledge Victoria Olowu, Marshé Edwards, Fred Park, Persus Akowuah, Salma Eltahir, Katherine Zhou, Domenic Tommarello, Pang-Ning Teng, Katlin Wilson, Sakiyah TaQee, and Tamara Abulez for histopathology and proteomic sample preparation and informatic analysis support.

Author Contributions: Contributed to conception: NWB, TPC. Contributed to experimental design: ALH, NWB, TPC. Contributed to identification and acquisition of the patient specimens: GG, DM, JO, GLM, TPC. Contributed to acquisition, analysis and/or interpretation of data: ALH, NWB, WB, SMM, BLH, KAC, MZ, VC, JL, TL, JO, DM, GG, CR, BB, UNMR, EFP, GLM, TPC. Drafted and/or revised the article: ALH, NWB, YC, KO, AKS, KMD, CDS, UNMR, MP, EFP, GLM, TPC. Acquired funding for the research: YC, GLM, TPC. All authors read and approved the final manuscript.

Declaration of Interests: TPC is a ThermoFisher Scientific, Inc SAB member and receives research funding from AbbVie. EFP receives research funding from Genentech, Pfizer, AbbVie, and is a co-inventor of the RPPA technology described herein and receives royalties on the related license agreements.

Disclaimer: The views expressed herein are those of the authors and do not reflect the official policy of the Department of Army/Navy/Air Force, Department of Defense, or U.S. Government.

Figure Legends

Figure 1. Study workflow. Illustration of histological tissue preparation, laser microdissection, proteomic analyses, and transcriptomic analysis (A), with representative pre- and post-LMD images from the top and bottom levels of the tissue from Case 343WM (B). (A) Specimen blocks obtained from 10 HGSOC patients were each cut into ~200 consecutive thin tissue sections (left panel), which were each laser microdissected for enrichment of discrete tumor epithelium, discrete stroma, or whole tumor collections (middle panel) for analysis via quantitative proteomics and transcriptomics (right panel). One case (343WM; middle panel, top) was uniquely used for laser microdissection (LMD) enrichment of four tumor epithelium cores with adjacent replicate regions from each of 100 or 50 slides evenly distributed through the depth of the specimen for MS proteomics or transcriptomics, respectively. For 343WM, additional sets of 9 slides from spatially separated levels within the specimen block were each discretely microdissected for all remaining tumor and stroma after collecting the cores by LMD, as well as a nearest neighboring whole tumor collection. The remainder of the specimen was cryopulverized in liquid nitrogen. The specimen blocks from the remaining 9 cases (middle panel, bottom) were divided into 5 levels (quintiles) of equal depth. Within each level, interlaced sections were used for LMD enrichment of discrete tumor epithelium, discrete stroma, and whole tumor collections for each downstream analytical purpose. Proteins and transcripts isolated from each of these distinct collections were analyzed by isobaric tagging and high-resolution liquid chromatography-tandem mass spectrometry, reverse phase protein microarray, and/or next generation sequencing. (B) Representative pre- and post-LMD images are shown for 343WM from tissue sections at the top and bottom levels used for proteomic analysis. The number in the

bottom right corner of each micrograph indicates the slide number shown. The scale bar in the bottom left corner of each micrograph indicates a length of 4 mm.

Figure 2. Unsupervised hierarchical cluster analysis of differentially abundant proteins and transcripts. (A) 1,928 differentially abundant proteins and (B) 3,861 transcripts with median absolute deviation (MAD)>0.5 from case 343WM, and (C) 6,199 differentially abundant proteins with MAD>1 in the expanded cohort (n=9). (C) Protein abundances are represented across n=123 samples derived from n=9 patients in the expanded cohort consisting of: LMD enriched tumor epithelium (n=45 total; 5 levels/patient), LMD enriched stroma (n=33 total; 2-5 levels/patient), and whole tumor (n=45 total; 5 levels/patient) samples. Highlighted box depicts the median tumor purity values from manual pathology review for each of the whole tumor collections as they appear in the heatmap, ordered from left to right. Dark elongated border line distinguishes the whole tumor collections which clustered with LMD enriched stroma (left) from those that clustered with LMD enriched tumor (right). Red and blue "X" marks represent interceding LMD enriched stroma or tumor collections, respectively.

Figure 3. Protein and transcript abundance of epithelial and stromal markers in HGSOC as well as cellular admixture analyses (xCell [13]). (A) Heatmaps depicting protein and transcript abundances and cellular admixture enrichment scores from 343WM for replicate tumor cores and by depth within the specimen block for LMD enriched tumor, stroma, and whole tumor collections. Protein abundance from the cryopulverized tumor is included. Size and color of each shape reflects Spearman correlation. (B) Boxplots depicting relative protein abundances for KRT19, CDH1, FAP, and VCAN and (C) cellular admixture scores in the expanded cohort

(n=9). ES= LMD enriched stroma; ET= LMD enriched tumor; WT= whole tumor. P-values with (*) indicate statistically significant differential expression ($p<0.0001$) between ES and ET.

Figure 4. Protein-RNA Spearman Correlation Matrix for case 343WM. Spearman correlation analysis of 5,742 genes that were co-measured as proteins and corresponding transcripts in 343WM. Size and color of each circle reflects Spearman correlation.

Figure 5. Protein and transcript abundance of markers correlating with prognostic molecular signatures of altered disease outcome in HGSOC. (A) Transcript abundances for markers correlated with suboptimal surgical debulking identified by Liu et al (2015) [24], and protein and transcript abundances correlating with prognostic molecular subtypes identified by Konecny et al (2014) [22] measured in 343WM. (B) Stacked bar graphs depicting the probability of each collection type (LMD enriched stroma, LMD enriched tumor, and whole tumor) per level per patient belonging to consensus molecular subtypes identified by Chen et al (2018) [4] based on protein abundance.

Figure 6. Patient-specific dendrograms depicting Spearman correlations between LMD enriched collections based on differentially expressed proteins. (A) Representative relatedness of all collection types from 343WM, including tumor cores, LMD enriched tumor epithelium, LMD enriched stroma, whole tumor, and cryopulverized tissue. (B) Relatedness of tumor cores versus LMD enriched tumor epithelium from 343WM. (C-F) Relatedness of LMD enriched tumor versus stroma from 343WM, 343WK, 343WQ, and 343WH, respectively. With the exception of the LMD enriched tumor cores vs LMD enriched tumor epithelium comparison

in panel B which was calculated using proteins with a median absolute deviation (MAD) >0.5, all comparisons in panels A and C-F were made using proteins with MAD >1. Comparisons marked with (*) indicate a significant difference ($p<0.01$) between groups, with p-values of 1.264E-05, 0.0012, 0.0003372, 0.00097, and 0.2205 for the comparisons in panels B-F, respectively. The yellow, blue, and red ovals in panels B-F highlight the clusters of LMD enriched tumor cores, tumor epithelium, and stroma, respectively.

Figure 7. Representative case (343WQ) depicting variable molecular expression and subtype classification by level. H&E images show the tissue sections mounted on glass slides bounding the top of each level. The tissue section number is notated in the bottom right corner of each micrograph. The median tumor cellularity with relative standard deviation (%CV), molecular subtype, and protein abundances of representative tumor and stroma markers present in the whole tumor collections are indicated for each level. The median tumor cellularity calculated from review of multiple images per level with the %CV included in parenthesis (from Supplemental Table 1) are reported as percentages. Correlations with consensus molecular subtypes (Figure 5B and Supplemental Table 28) are shown. The Log_2-transformed protein abundances are shown for tumor/epithelial markers (CDH1 and KRT19) and stroma markers (FAP and VCAN) (from Supplemental Table 7).

Supplemental Table Legends

Supplemental Table 1. Clinical features and manual pathology assessment of tumor purity throughout the depth of the HGSOC patient specimen block. Representative H&E stained glass slides from were examined at ~200 µm intervals for case 343WM or ~100 µm intervals for the additional 9 cases by a board-certified pathologist for percent by area estimation of tumor cellularity, necrosis, stroma, normal ovarian epithelium, lymphocytes, and polymorphonuclear leukocytes (PMN). Multiple images per level per case were reviewed and the median tumor cellularity and median stroma cellularity are reported with corresponding percent coefficient of variation (%CV) reported in parentheses. Abbreviations: NACT= neoadjuvant chemotherapy; FT= fallopian tube; Ov= ovary; ca= cancer; NOS= not otherwise specified.

Supplemental Table 2. Depiction of full study cohort. Numerical values indicate the number of LMD tissue sections that were used for each collection.

Supplemental Table 3. LMD enriched tumor epithelium and stroma cell areas acquired by laser microdissection and automated analyses of collected regions of interest (ROI). ROI are denoted as millimeter squared (mm^2) areas, cell nuclei as μm^2 areas or as total cell counts derived from cellular nuclei measured in LMD enriched tumor or stroma ROIs.

Supplemental Table 4. TMT Plexing Strategy. For 343WM, tryptic peptides were labeled with isobaric Tandem Mass Tags (TMT) according to the manufacturer's instructions using the TMT 10-Plex Kit from Thermo Fisher for a total of 4 plexes. 30 µg peptides from the 8 cores, 9 non-discrete whole tumor collections, and cryopulverized tissue sample were individually mixed with

respective TMT reagents for 1 h at room temperature, then quenched using 5% hydroxylamine. 10 μg peptides/sample were similarly TMT labeled from the 9 discrete collections each of remaining LMD-enriched tumor epithelium or stroma.

For the remaining 9 cases, digested peptide samples were labeled in patient-specific plexes using the TMTpro 16-Plex Kit (Thermo Fisher). Specifically, 5 μg peptide from up to 5 levels/patient each of LMD enriched tumor epithelium, LMD enriched stroma, and whole tumor collections were incubated with the TMTpro reagents per plex for a total of 80 μg/plex and 1 plex/patient. To replace samples from which <5 μg peptide was recovered, empty TMT channels were filled using equal amounts of peptide mixed from each of the 5 levels of the whole tumor collections.

Supplemental Table 5. Global protein matrix. Log_2 transformed fold-change abundances of 6,053 proteins imputed across all samples measured in case 343WM.

Supplemental Table 6. Global transcriptome matrix. Normalized abundances of 20,535 RNA transcripts measured in case 343WM calculated relative to the average RPM abundance quantified across all samples for a given transcript, as reported by the Torrent Suite (v5.8.0) software, before Log_2 fold-change transformation.

Supplemental Table 7. **Global protein matrix for expanded cohort (n=9 patients).** Log_2 transformed fold-change abundances of 6,199 proteins imputed across all samples (n=123).

Supplemental Table 8. Global transcriptome matrix for expanded cohort (n=2 patients). Normalized abundances of 19,758 RNA transcripts calculated relative to the average RPM abundance quantified across all samples (n=6) for a given transcript, as reported by the Torrent Suite (v5.8.0) software, before Log_2 fold-change transformation.

Supplemental Table 9. Unsupervised analysis of protein abundance (median absolute deviation > 0.5) measured in case 343WM.

Supplemental Table 10. Unsupervised analysis of transcript abundance (Log_2 fold-change abundances with median absolute deviation > 0.5) measured in case 343WM.

Supplemental Table 11. Unsupervised analysis of protein abundance (median absolute deviation > 1) measured in the expanded cohort (n=9 cases).

Supplemental Table 12. Unsupervised analysis of transcript abundance (median absolute deviation > 1) measured in the expanded cohort (n=2 cases).

Supplemental Table 13. Cell type enrichment analyses as performed using RPM-level RNA-Seq data for case 343WM and default settings in xCell (http://xcell.ucsf.edu/, [60]).

Supplemental Table 14. Cell type enrichment analyses as performed using protein-level TMT LC-MS/MS data from the expanded cohort (n=9 cases) and default settings in xCell (http://xcell.ucsf.edu/, [60]).

Supplemental Table 15. Median absolute deviation (MAD) of LMD-enriched samples expressing or lacking signal peptide sequences and extracellular classification (n=4 cases). P-values indicate the reliability of the presence or absence of a signal peptide or extracellular classification within the indicated LMD-enriched tissue across all levels/case. 9 levels were used for comparison for case 343WM, while 5 levels/case were used each for cases 343WK, 343WQ, and 343WH.

Supplemental Table 16. Co-quantified proteins and transcripts from case 343WM. Log_2 transformed fold-change abundances of 5,742 imputed proteins that were co-measured at the transcriptome level from case 343WM.

Supplemental Table 17. Co-quantified proteins and transcripts in the expanded cohort (n=2 patients). Log_2 transformed fold-change abundances of 5,379 imputed proteins that were co-measured at the transcriptome level.

Supplemental Table 18. Information for all antibodies used for RPPA analysis.

Supplemental Table 19. RPPA abundance values for protein and phosphoprotein targets in LMD enriched tumor, LMD enriched stroma, and whole tumor samples from n=9 HGSOC cases.

Supplemental Table 20. Spearman correlations for proteins measured by TMT LC-MS/MS and RPPA.

Supplemental Table 21. Top altered canonical pathways in laser microdissection-enriched tumor epithelium versus stroma identified using Ingenuity Pathway Analysis. Comparison of the most differential pathways and diseases/functions between LMD enriched tumor and stroma was determined using pairwise supervised analysis of proteomic and transcriptomic data with LIMMA adjusted p-value < 0.01 exhibiting a Log_2 fold-change cut-off ± 1.

Supplemental Table 22. Top altered diseases and functions in laser microdissection-enriched tumor epithelium versus stroma identified using Ingenuity Pathway Analysis. Comparison of the most differential diseases/functions between LMD enriched tumor and stroma was determined using pairwise supervised analysis of proteomic and transcriptomic data with LIMMA adjusted p-value < 0.01 exhibiting a Log_2 fold-change cut-off ± 1.

Supplemental Table 23. Significantly differentially expressed transcript alterations between LMD enriched tumor epithelium versus stroma from case 343WM identified using Ingenuity Pathway Analysis (IPA) of known gene targets of FDA-approved anticancer drugs. Comparison of prevalent drug targets present in LMD enriched tumor versus stroma was determined using pairwise supervised analysis of proteomic and transcriptomic data with LIMMA adjusted p-value < 0.01 exhibiting a Log_2 fold-change cut-off ± 1. The complete list of all differentially expressed genes that are known drug targets from our proteomic-level and

transcriptomic-level data was compared with a list of 150 FDA-approved anticancer drugs as of 2014 analyzed in a study by Sun et al [21].

Supplemental Table 24. Proteomic-level data for 381 proteins which displayed the same pattern of enrichment across all 9 cases and which had Log_2 fold-changes > ±1 used as input for Ingenuity Pathway Analysis.

Supplemental Table 25. Top altered canonical pathways in laser microdissection-enriched tumor epithelium versus stroma in the expanded cohort (n=9 cases) identified using Ingenuity Pathway Analysis. Comparison of the most differential canonical pathways between LMD enriched tumor and stroma was determined using unsupervised analysis of 381 proteins which displayed the same direction of enrichment in all 9 patients with LIMMA adjusted p-value < 0.01 exhibiting a Log_2 fold-change cut-off ± 1.

Supplemental Table 26. Top altered diseases and biofunctions in laser microdissection-enriched tumor epithelium versus stroma in the expanded cohort (n=9 cases) identified using Ingenuity Pathway Analysis. Comparison of the most differential diseases/functions between LMD enriched tumor and stroma was determined using unsupervised analysis of 381 proteins which displayed the same direction of enrichment in all 9 patients with LIMMA adjusted p-value < 0.01 exhibiting a Log_2 fold-change cut-off ± 1.

Supplemental Table 27. Significantly differentially expressed alterations between LMD enriched tumor epithelium versus stroma in the expanded cohort (n=9 cases) identified using Ingenuity Pathway Analysis (IPA) of known gene targets of FDA-approved anticancer drugs. Comparison of prevalent drug targets present in LMD enriched tumor versus stroma was determined using unsupervised analysis of 381 proteins which displayed the same direction of enrichment in all 9 patients with LIMMA adjusted p-value < 0.01 exhibiting a Log_2 fold-change cut-off ± 1. The complete list of all differentially expressed genes that are known drug targets from our proteomic-level and transcriptomic-level data was compared with a list of 150 FDA-approved anticancer drugs as of 2014 analyzed in a study by Sun et al [21].

Supplemental Table 28. Probabilities for correlation of 343WM samples with consensus molecular subtypes using the consensusOV package in R [4].

Supplemental Table 29. Probabilities for correlation of samples from the expanded cohort (n=9) with consensus molecular subtypes using the consensusOV package in R [4].

Supplemental Table 30. Dendrogram Spearman correlations.

Supplemental Table 31. The top 5 ranked most and least variable proteins from genes measured in a clinical setting. A composite list of 70 genes and/or proteins that were examined in the clinical setting for cases 343WP, 343WN, and 343WQ was generated, and variability of

1083 protein expression in cases 343WK, 343WQ, and 343WH, for which the full complement of 5
1084 levels/case for each LMD enriched tumor, LMD enriched stroma, and whole tumor were
1085 available in our proteomic dataset. Relative standard deviation (RSD) values of protein
1086 expression were calculated between the 5 levels within each collection type within a patient's
1087 samples and then ranked. The median rank and median RSD between patients for the top 5 most
1088 and least variable proteins within each patients' samples are shown.

Supplemental Figure Legends

Supplemental Figure 1. Detailed study workflow diagram. Illustration of histological tissue preparation and laser microdissection (A), isobaric tagging and high-resolution liquid chromatography-tandem mass spectrometry (TMT LC-MS/MS) analysis (B), reverse phase protein microarray (RPPA) analysis (C), and transcriptomic (RNA-seq) analysis (D). (A) Specimen blocks obtained from 10 HGSOC patients were each cut into ~200 consecutive thin tissue sections (left panel), which were each laser microdissected for enrichment of discrete tumor epithelium, discrete stroma, or whole tumor collections (middle panel) for analysis via quantitative proteomics and transcriptomics (right panel). One case (343WM; middle panel, top) was uniquely used for laser microdissection (LMD) enrichment of four tumor epithelium cores with adjacent replicate regions from each of 100 or 50 slides evenly distributed through the depth of the specimen for MS proteomics or transcriptomics, respectively. For 343WM, additional sets of 9 slides from spatially separated levels within the specimen block were each discretely microdissected for all remaining tumor and stroma after collecting the cores by LMD, as well as a nearest neighboring whole tumor collection. The remainder of the specimen was cryopulverized in liquid nitrogen. The specimen blocks from the remaining 9 cases (middle panel, bottom) were divided into 5 levels (quintiles) of equal depth. Within each level, interlaced sections were used for LMD enrichment of discrete tumor epithelium, discrete stroma, and whole tumor collections for each downstream analytical purpose. Proteins and transcripts isolated from each of these distinct collections were analyzed by TMT LC-MS/MS (B), RPPA (C), and/or next generation sequencing (D). (B) The LMD tissue for mass spectrometry-based analysis was digested using pressure cycling technology, and digested peptides were then quantified and TMT-labeled. 10 μg/sample from case 343WM were labeled using TMT-10 plex reagents for a

total of 4 TMT plexes. 5 µg/sample from the additional 9 cases were labeled using the TMTpro 16-plex reagents in patient-specific plexes. Individually labeled samples were then pooled, fractionated via basic reversed-phase liquid chromatography (bRPLC), pooled into 36 or 24 combined fractions for case 343WM or the remaining 9 cases, respectively, and pooled fractions were analyzed via LC-MS/MS. (C) LMD tissue for RPPA was collected into a tissue lysis buffer, and cell lysates were prepared for microarray printing. Samples arrayed in technical replicates (triplicates) were stained using 281 antibodies targeting native and post-translationally modified proteins. Immunostained arrays were imaged, signals were normalized relative to stained control slides, and analyzed. (D) LMD tissue for RNA-seq was collected into a lysis buffer for extraction and subsequent purification and quantification of RNA. Quality of the isolated RNA was measured. RNA samples were then reverse transcribed into cDNA and individually labeled with IonCode barcode sequences. cDNA libraries containing 5-6 LMD samples/library, plus a universal human reference RNA sample, and 1-2 control water blanks were cleaned using solid phase reversible immobilization (SPRI) to remove fragments less than 100 bp and quantified via qPCR. Library concentration was adjusted to 100 pM and used for templating and chip-loading for RNA-seq. Genes were mapped to the hg19 human reference transcriptome.

Supplemental Figure 2. Unsupervised hierarchical cluster analysis of 874 transcripts with MAD>1 in the expanded cohort. Transcript abundances are represented across n=6 samples derived from n=2 patients in the expanded cohort consisting of: LMD enriched tumor epithelium, LMD enriched stroma, and whole tumor samples each taken from 1 level/patient.

Supplemental Figure 3. Boxplots depicting relative protein abundance for MUC16 in the expanded cohort. ES= LMD enriched stroma; ET= LMD enriched tumor; WT= whole tumor. No significant difference between ES and ET (p-value= 0.08256807).

Supplemental Figure 4. Protein-RNA Spearman Correlation Matrix for cases 343WB and 343WH. Spearman correlation analysis of 5,379 genes that were co-measured as proteins and corresponding transcripts in 343WM.

Supplemental Figure 5. Correlation matrices of proteins co-quantified by TMT LC-MS/MS and RPPA proteomics. Spearman correlation analysis of 5,379 genes that were co-measured as proteins by TMT LC-MS/MS and RPPA for (A) LMD enriched tumor, (B) LMD enriched stroma, and (C) whole tumor.

Supplemental Figure 6. Transcript abundance of markers measured in 343WM correlating with a prognostic molecular signature of suboptimal cytoreduction in HGSOC identified by Liu et al. (2015) [24].

Supplemental Figure 7. Cancer-specific clinical histories for cases 343WP, 343WN, and 343WQ. Graphs represent a timeline of each patient's clinical history from time of diagnosis (Dx) to time of death or last follow-up and associated CA-125 levels. Brief descriptive patient histories are reported in the grey box. Dates of serial computerized tomography (CT) scans are

1155 shown as purple arrows. Dates of clinical events of diagnosis, progression recurrence, and final
1156 survival status are indicated by blue arrows and are detailed in the blue box. Dates of surgical
1157 and/or therapeutic interventions are indicated as light green arrows and are detailed in the light
1158 green box. Residual disease status following surgical debulking is indicated in orange boxes. The
1159 date acquired and tissue site for the specimens used in this study are notated in the black boxes
1160 associated with the primary debulking surgery (PDS). Dates of sample acquisition for
1161 examination of clinical marker expression and/or mutation status are indicated as dark green
1162 arrows; details of the company who analyzed the sample, the sample source (tissue or biofluid),
1163 and markers examined are listed in the CLIA test box(es) in the top right.

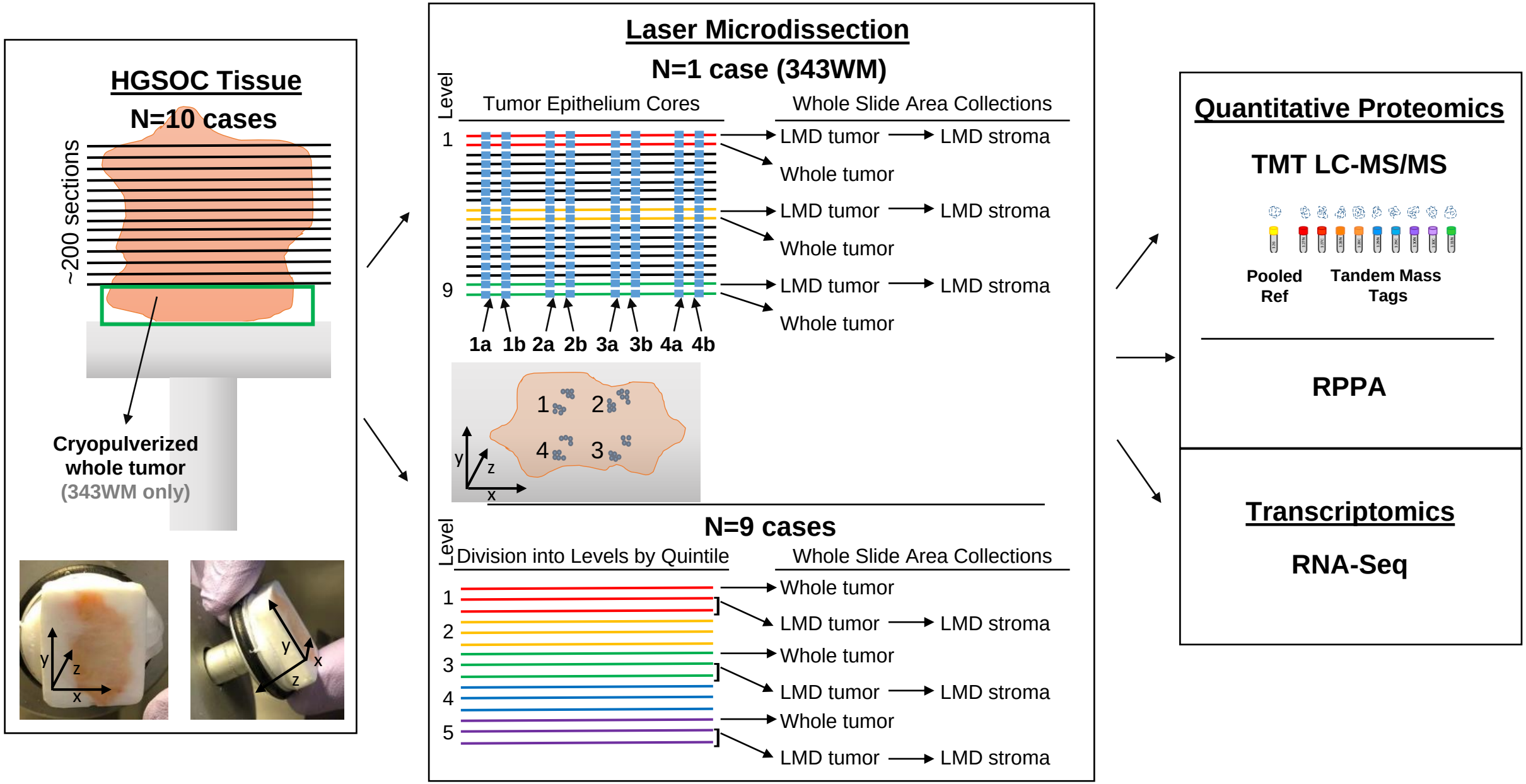
HGSOC Tissue
N=10 cases
~200 sections
Cryopulverized whole tumor
(343WM only)
y
z
x
Laser Microdissection
N=1 case (343WM)
Level
Tumor Epithelium Cores
Whole Slide Area Collections
1
9
LMD tumor
LMD stroma
Whole tumor
1a 1b 2a 2b 3a 3b 4a 4b
1
2
3
4
N=9 cases
Division into Levels by Quintile
Whole Slide Area Collections
1
2
3
4
5
Quantitative Proteomics
TMT LC-MS/MS
Pooled Ref
Tandem Mass Tags
RPPA
Transcriptomics
RNA-Seq

Figure 1A

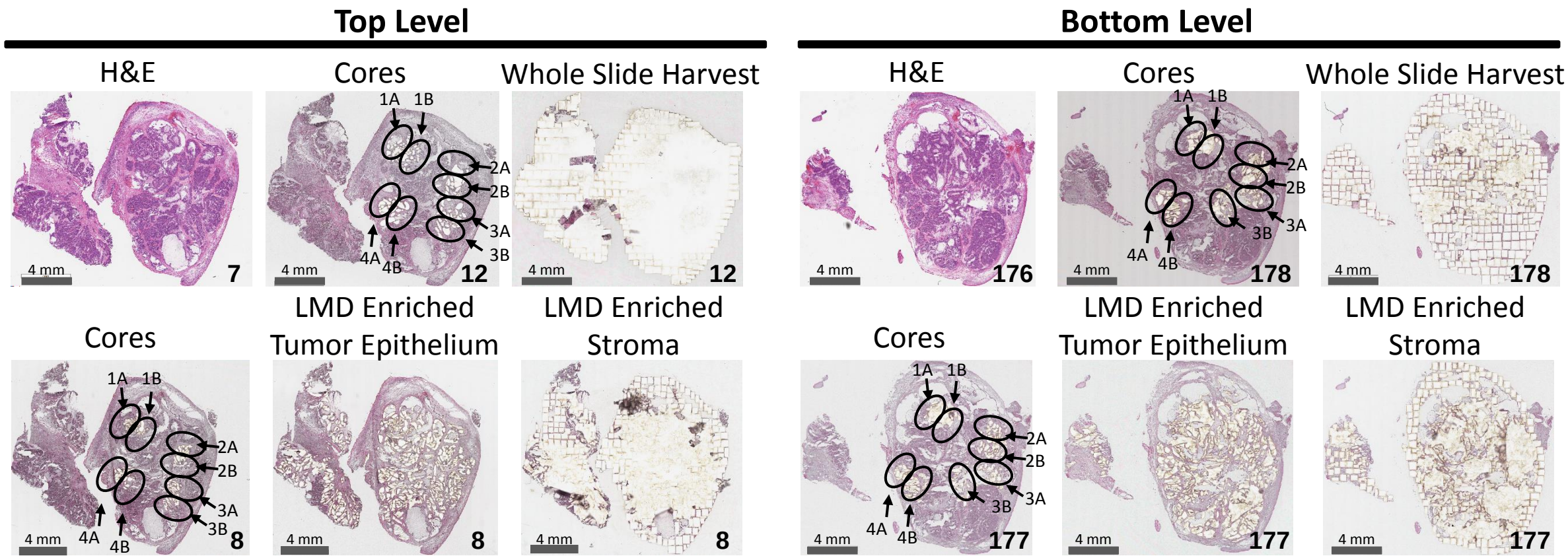
Top Level
H&E
Cores
Whole Slide Harvest
1A 1B
2A
2B
3A
3B
4A 4B
4 mm
7
12
12
Cores
LMD Enriched Tumor Epithelium
LMD Enriched Stroma
8
8
8
Bottom Level
H&E
Cores
Whole Slide Harvest
176
178
178
Cores
LMD Enriched Tumor Epithelium
LMD Enriched Stroma
177
177
177

Figure 1B

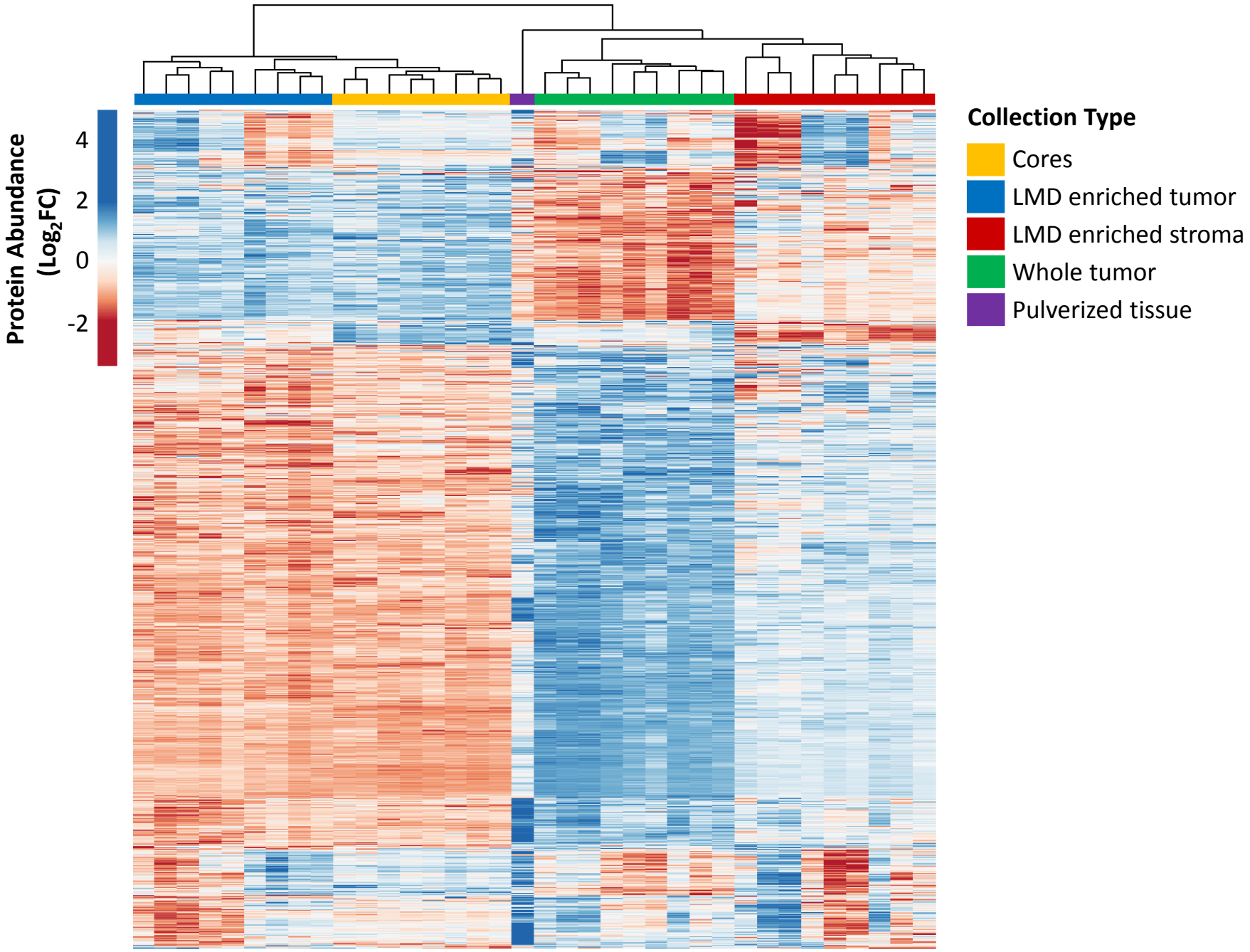
Protein Abundance
(Log2FC)
4
2
0
-2
Collection Type
Cores
LMD enriched tumor
LMD enriched stroma
Whole tumor
Pulverized tissue

Figure 2A

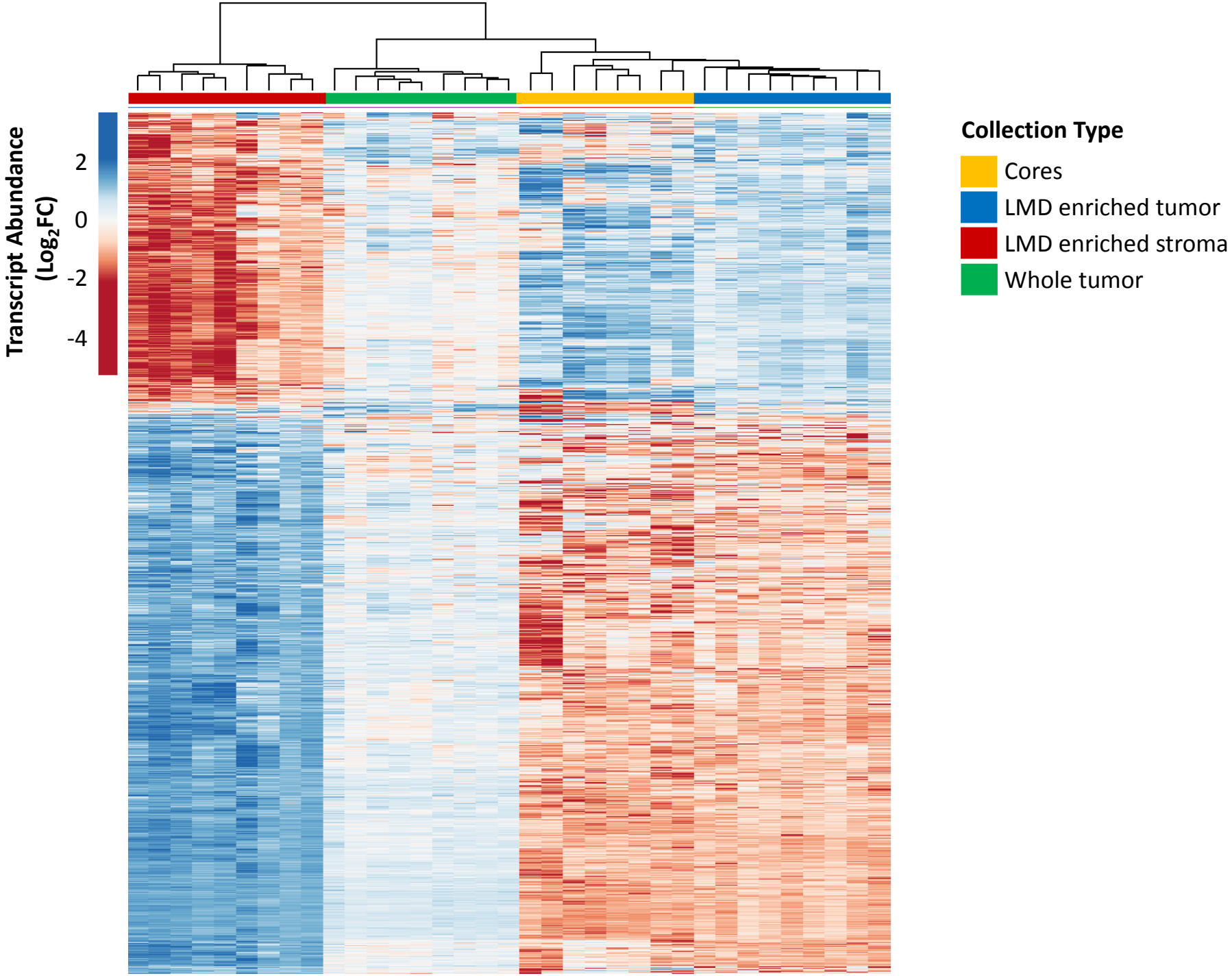
Transcript Abundance
(Log2FC)
2
0
-2
-4
Collection Type
Cores
LMD enriched tumor
LMD enriched stroma
Whole tumor

Figure 2B

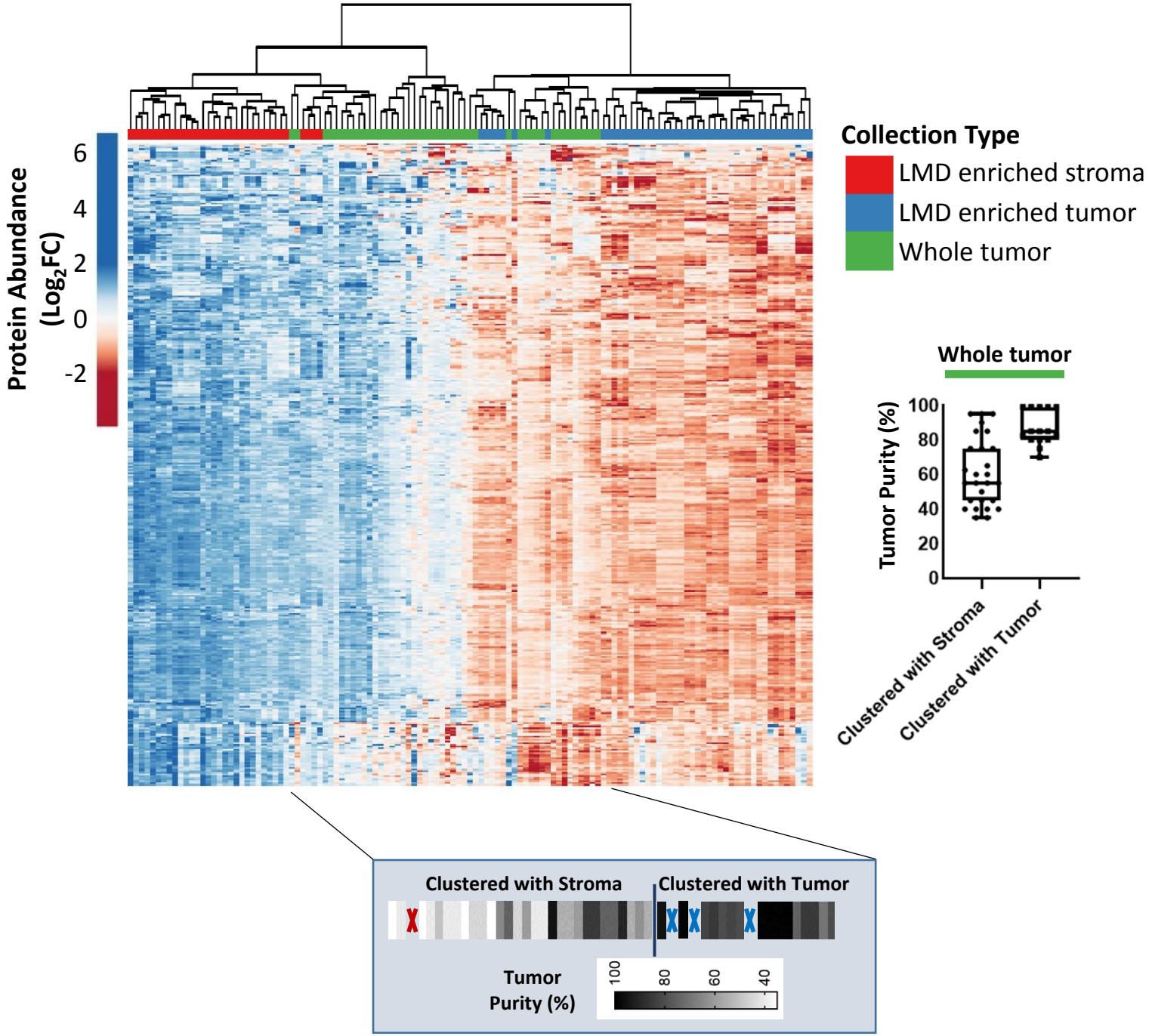
Protein Abundance
(Log2FC)
6
4
2
0
-2
Collection Type
LMD enriched stroma
LMD enriched tumor
Whole tumor
Whole tumor
Tumor Purity (%)
100
80
60
40
20
0
Clustered with Stroma
Clustered with Tumor
Clustered with Stroma
Clustered with Tumor
Tumor
Purity (%)
100
80
60
40

Figure 2C

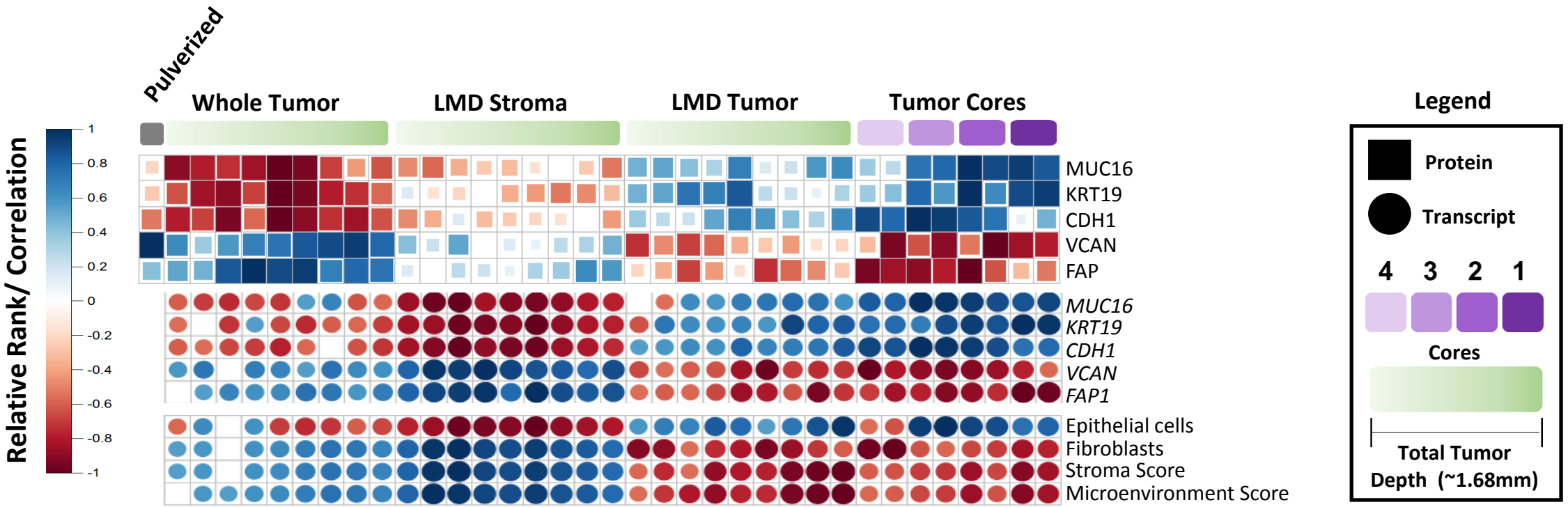
Pulverized
Whole Tumor
LMD Stroma
LMD Tumor
Tumor Cores
Relative Rank/ Correlation
1
0.8
0.6
0.4
0.2
0
-0.2
-0.4
-0.6
-0.8
-1
MUC16
KRT19
CDH1
VCAN
FAP
MUC16
KRT19
CDH1
VCAN
FAP1
Epithelial cells
Fibroblasts
Stroma Score
Microenvironment Score
Legend
Protein
Transcript
4 3 2 1
Cores
Total Tumor Depth (~1.68mm)

Figure 3A

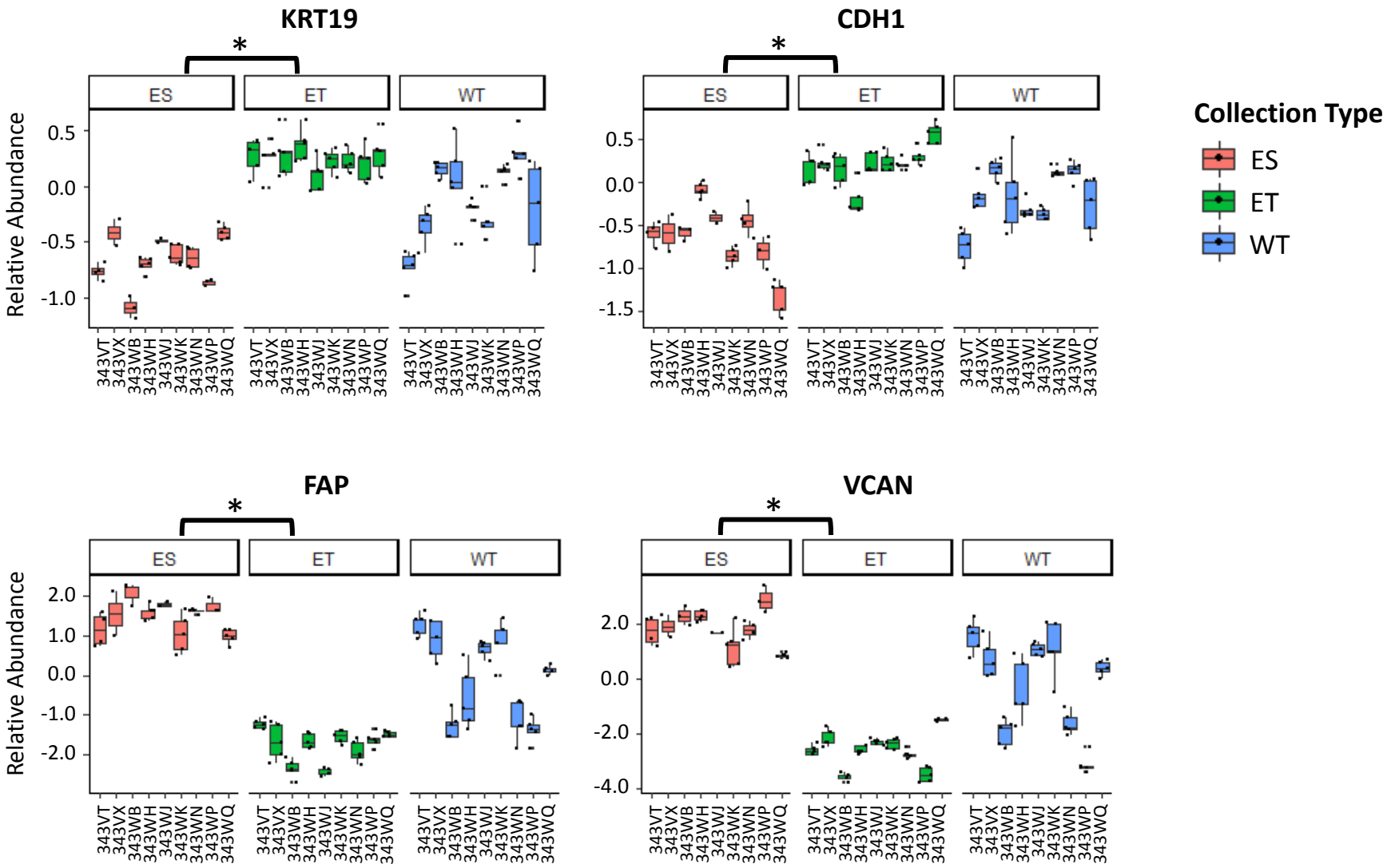
KRT19
CDH1
FAP
VCAN
*
ES
ET
WT
Relative Abundance
343VT
343VX
343WB
343WH
343WJ
343WK
343WN
343WP
343WQ
Collection Type
ES
ET
WT

Figure 3B

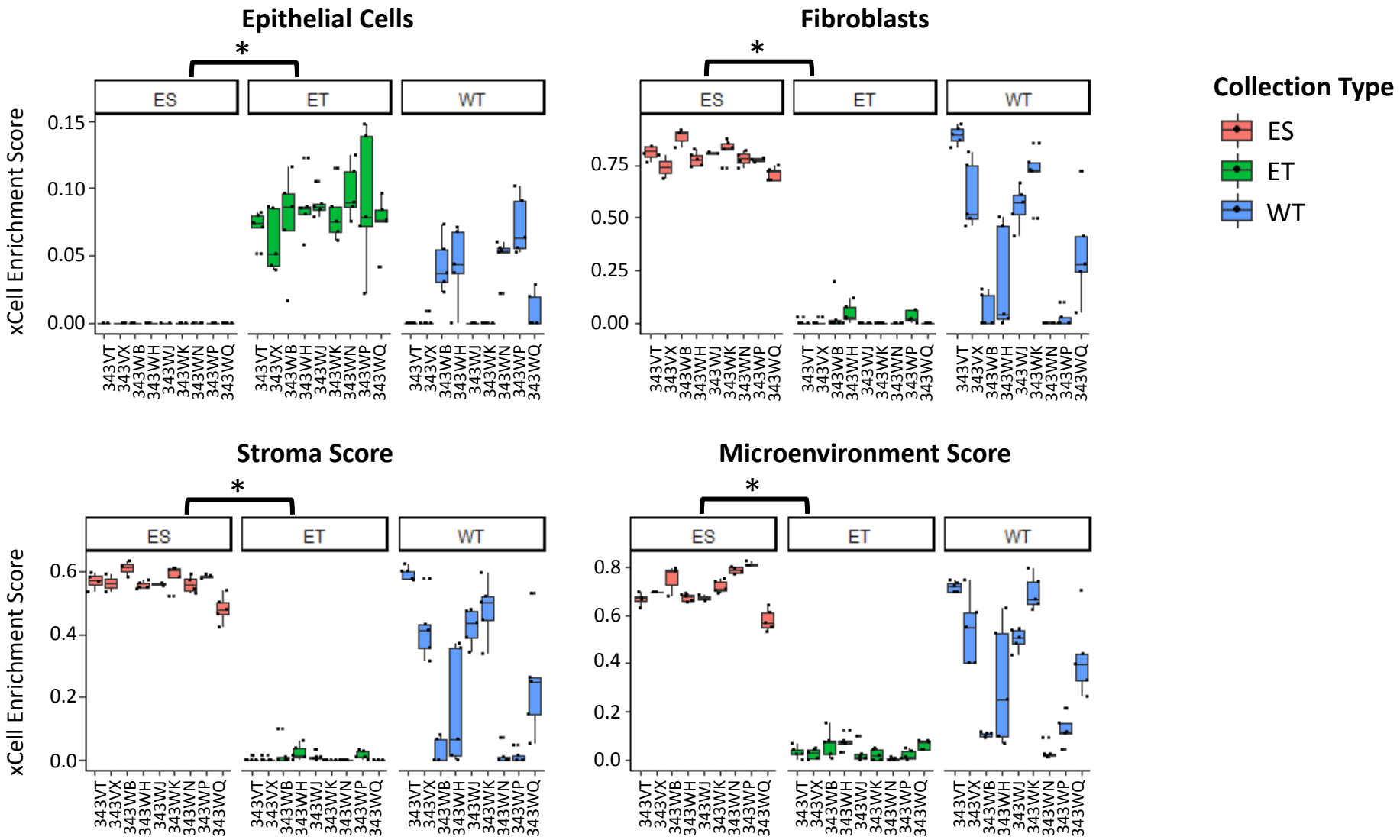
Epithelial Cells
Fibroblasts
Stroma Score
Microenvironment Score
xCell Enrichment Score
ES
ET
WT
*
343VT
343VX
343WB
343WH
343WJ
343WK
343WN
343WP
343WQ
Collection Type
ES
ET
WT

Figure 3C

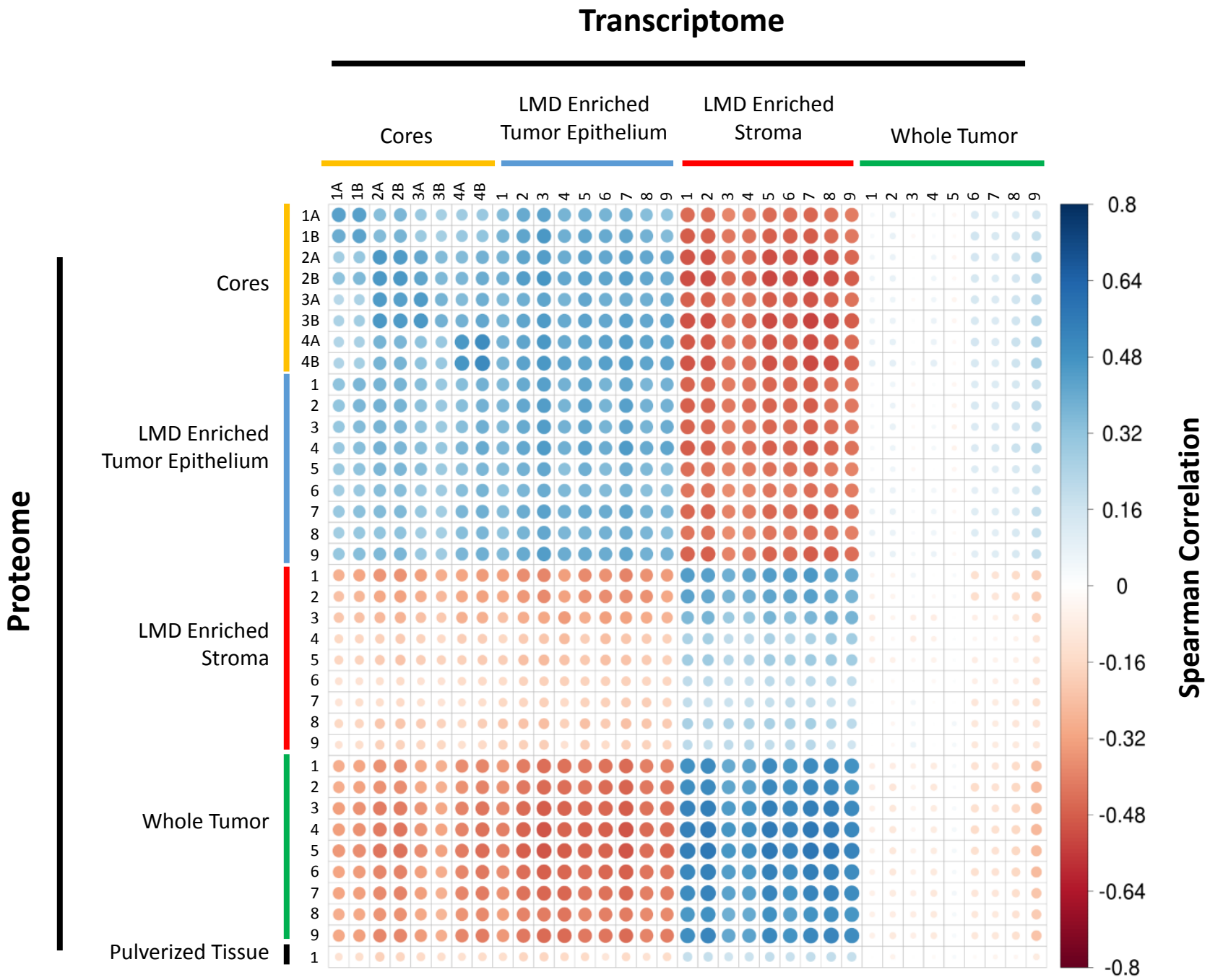
Transcriptome
Cores
LMD Enriched Tumor Epithelium
LMD Enriched Stroma
Whole Tumor
Proteome
Cores
LMD Enriched Tumor Epithelium
LMD Enriched Stroma
Whole Tumor
Pulverized Tissue
1A 1B 2A 2B 3A 3B 4A 4B
1 2 3 4 5 6 7 8 9
Spearman Correlation
0.8
0.64
0.48
0.32
0.16
0
-0.16
-0.32
-0.48
-0.64
-0.8

Figure 4

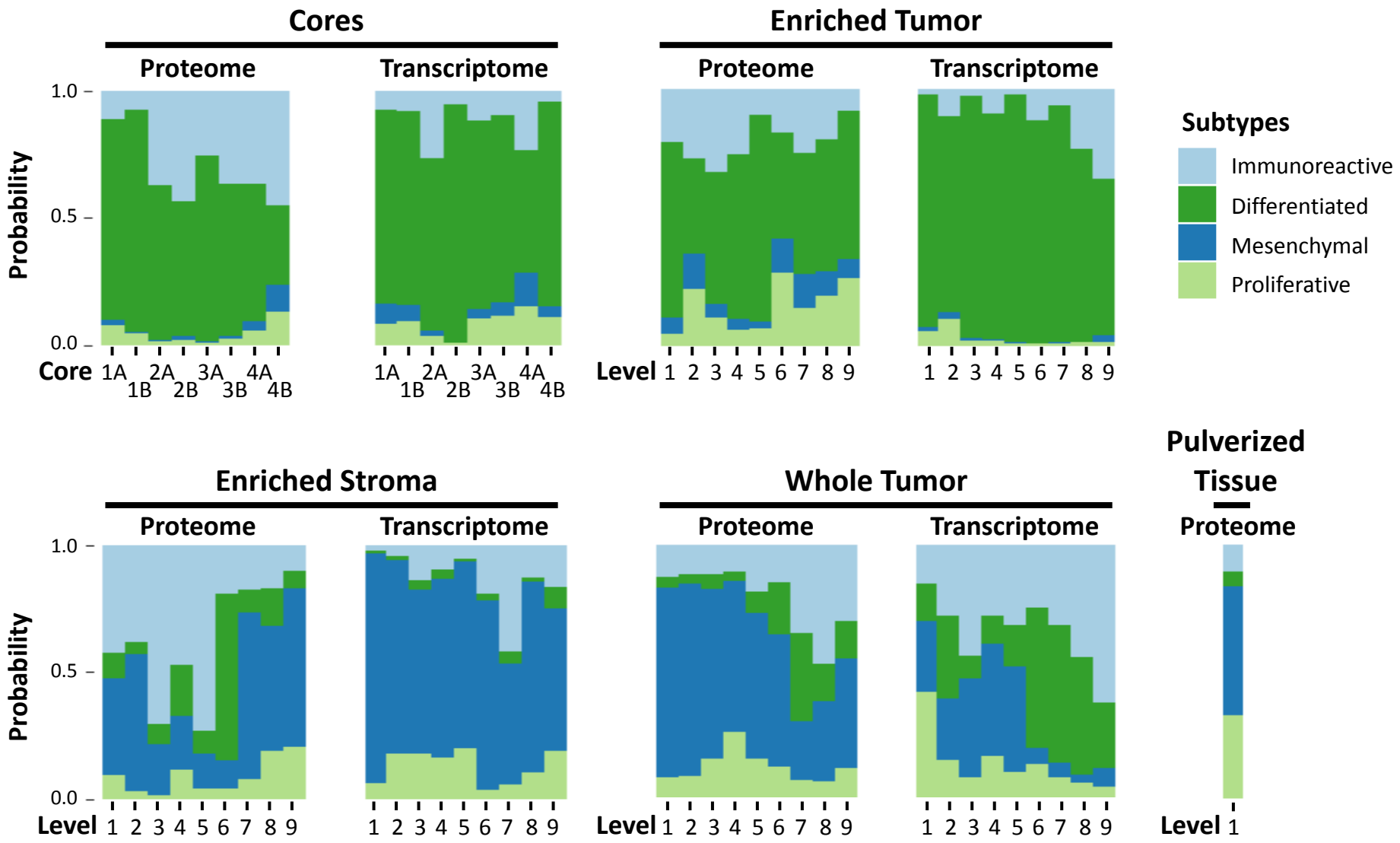
Cores
Proteome
Transcriptome
Enriched Tumor
Proteome
Transcriptome
Probability
1.0
0.5
0.0
Core 1A 1B 2A 2B 3A 3B 4A 4B
1A 1B 2A 2B 3A 3B 4A 4B
Level 1 2 3 4 5 6 7 8 9
1 2 3 4 5 6 7 8 9
Subtypes
Immunoreactive
Differentiated
Mesenchymal
Proliferative
Enriched Stroma
Proteome
Transcriptome
Whole Tumor
Proteome
Transcriptome
Pulverized Tissue
Proteome
Level 1

Figure 5A

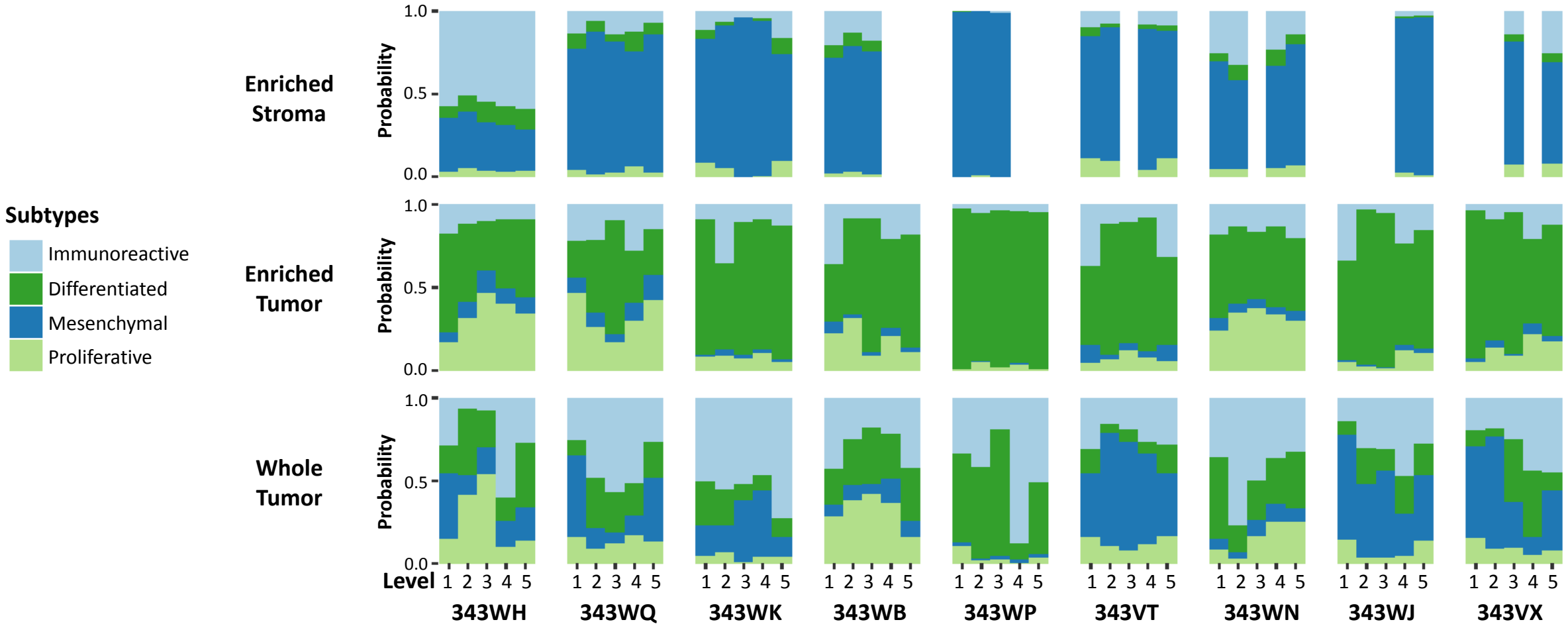
Subtypes
Immunoreactive
Differentiated
Mesenchymal
Proliferative
Enriched Stroma
Enriched Tumor
Whole Tumor
Probability
1.0
0.5
0.0
Level
1 2 3 4 5
343WH
343WQ
343WK
343WB
343WP
343VT
343WN
343WJ
343VX

Figure 5B

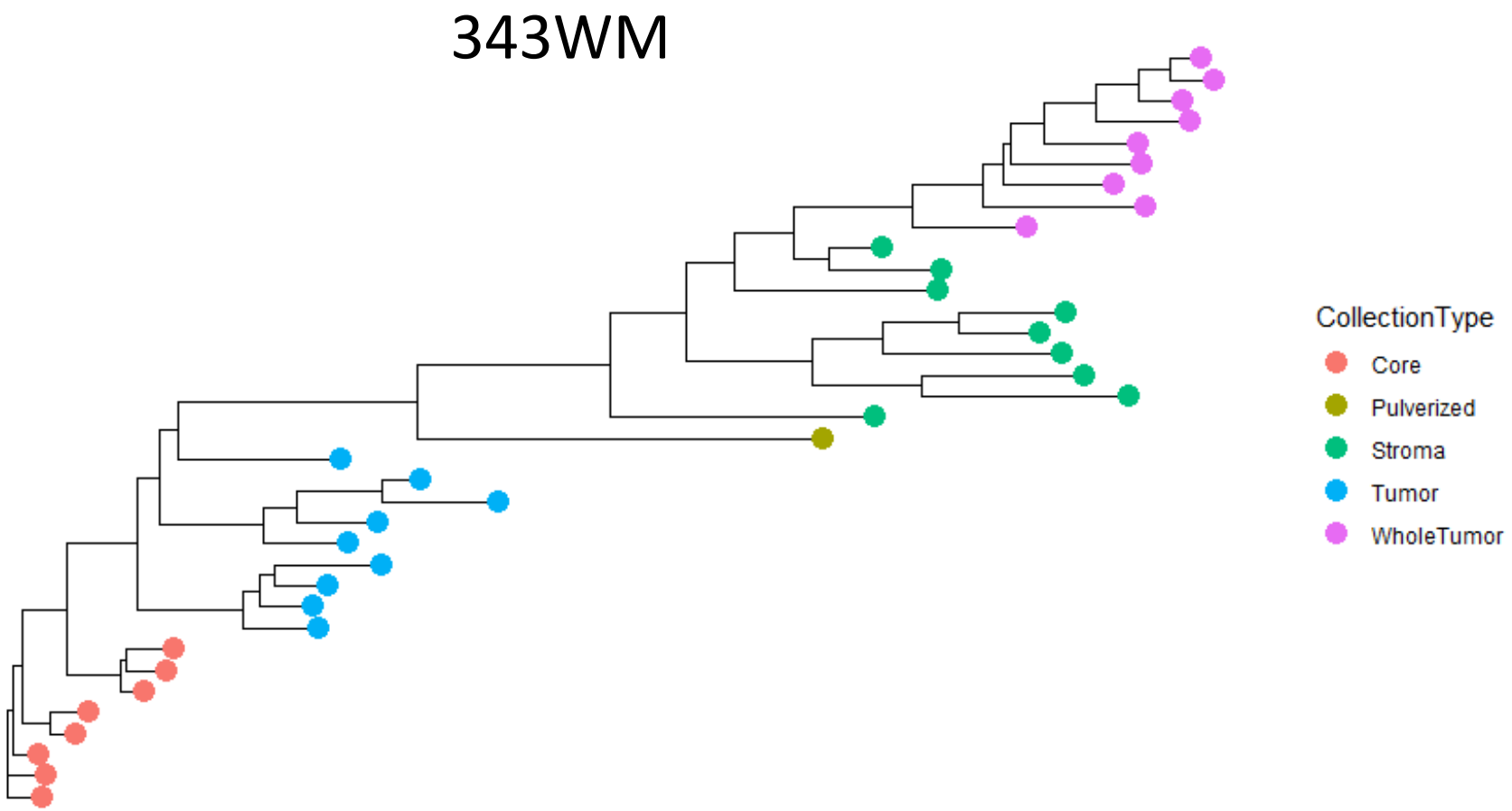
343WM
CollectionType
Core
Pulverized
Stroma
Tumor
WholeTumor

Figure 6A

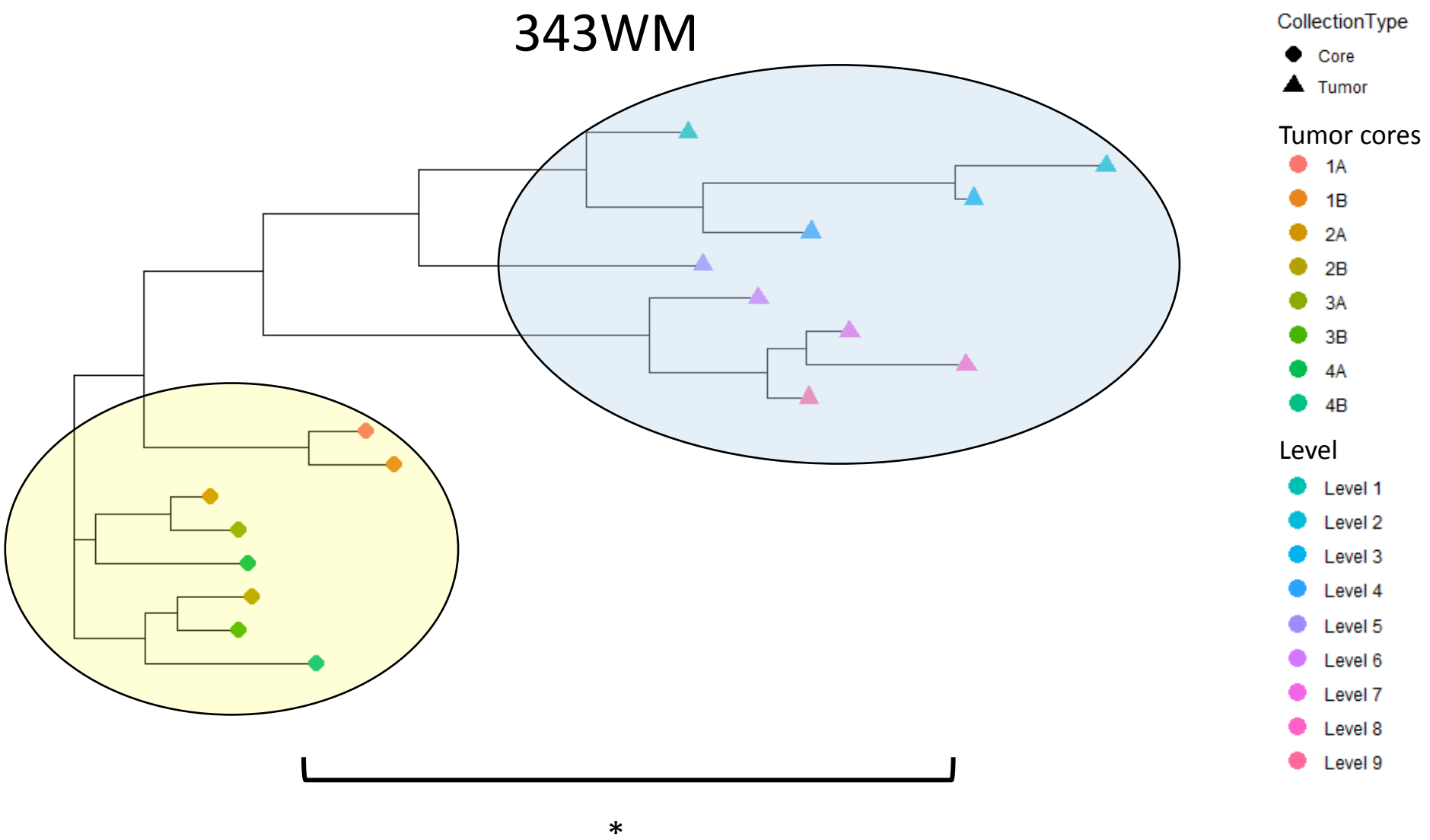
343WM
CollectionType
Core
Tumor
Tumor cores
1A
1B
2A
2B
3A
3B
4A
4B
Level
Level 1
Level 2
Level 3
Level 4
Level 5
Level 6
Level 7
Level 8
Level 9
*

Figure 6B

343WM

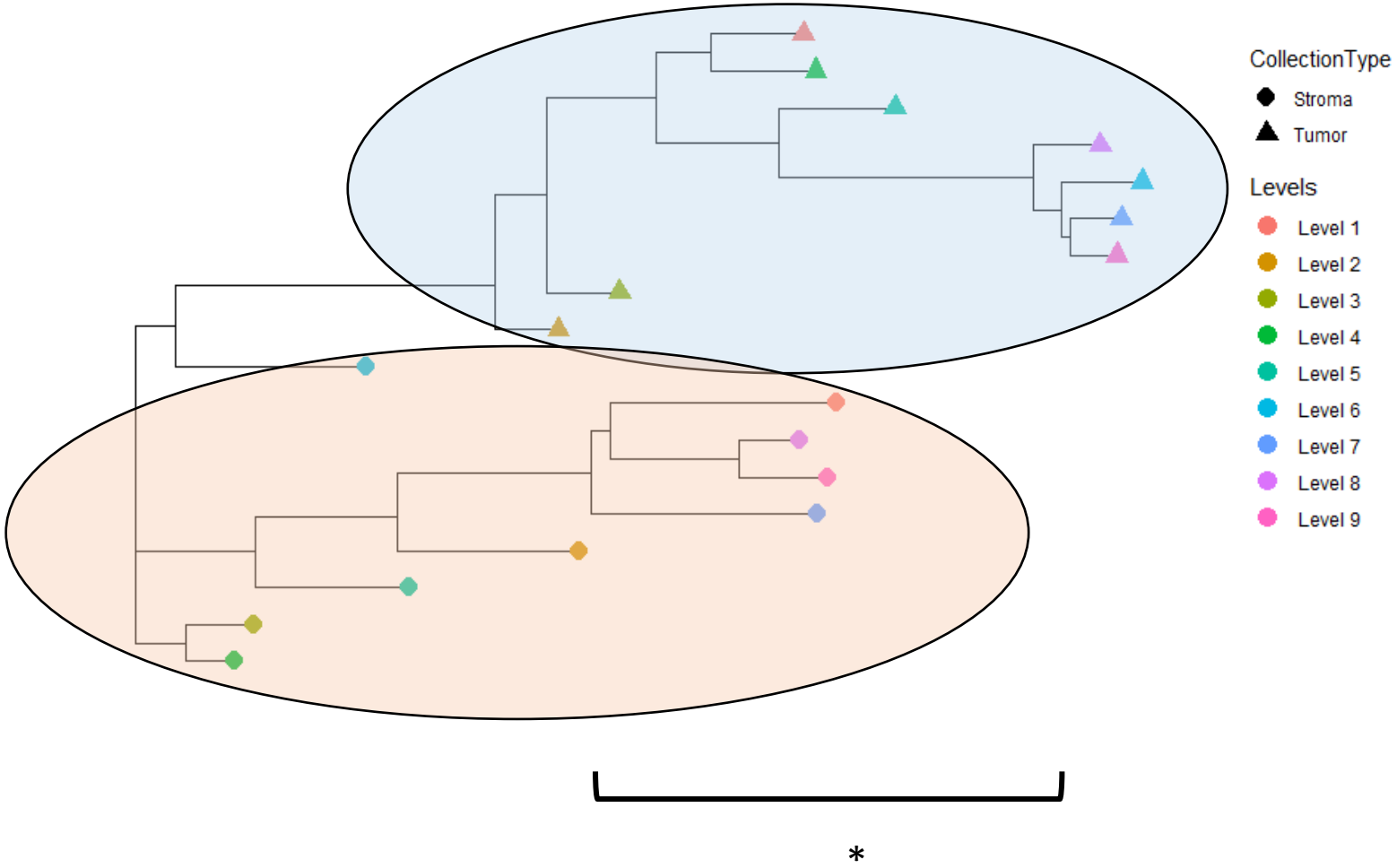

Figure 6C

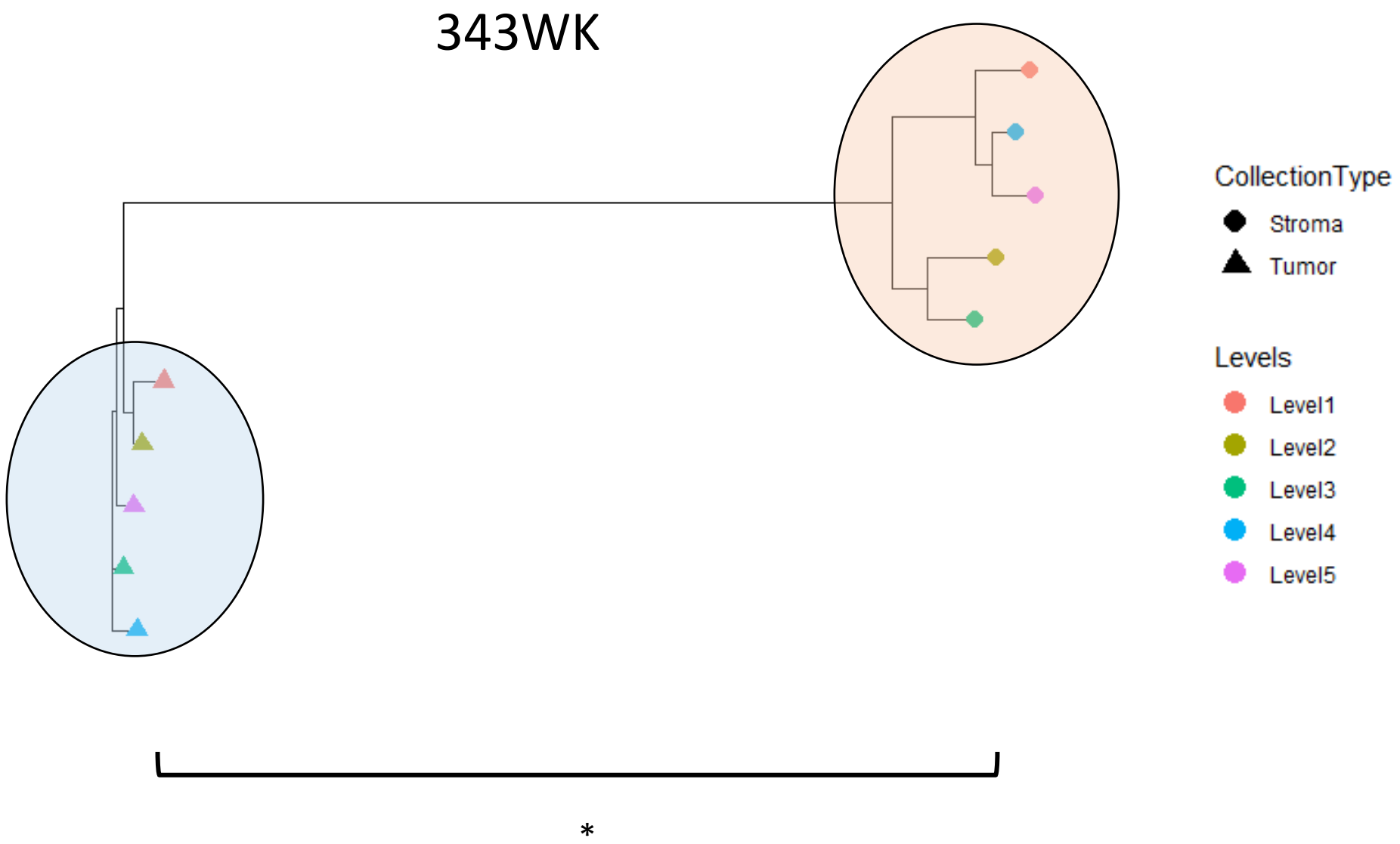
343WK
CollectionType
Stroma
Tumor
Levels
Level1
Level2
Level3
Level4
Level5
*

Figure 6D

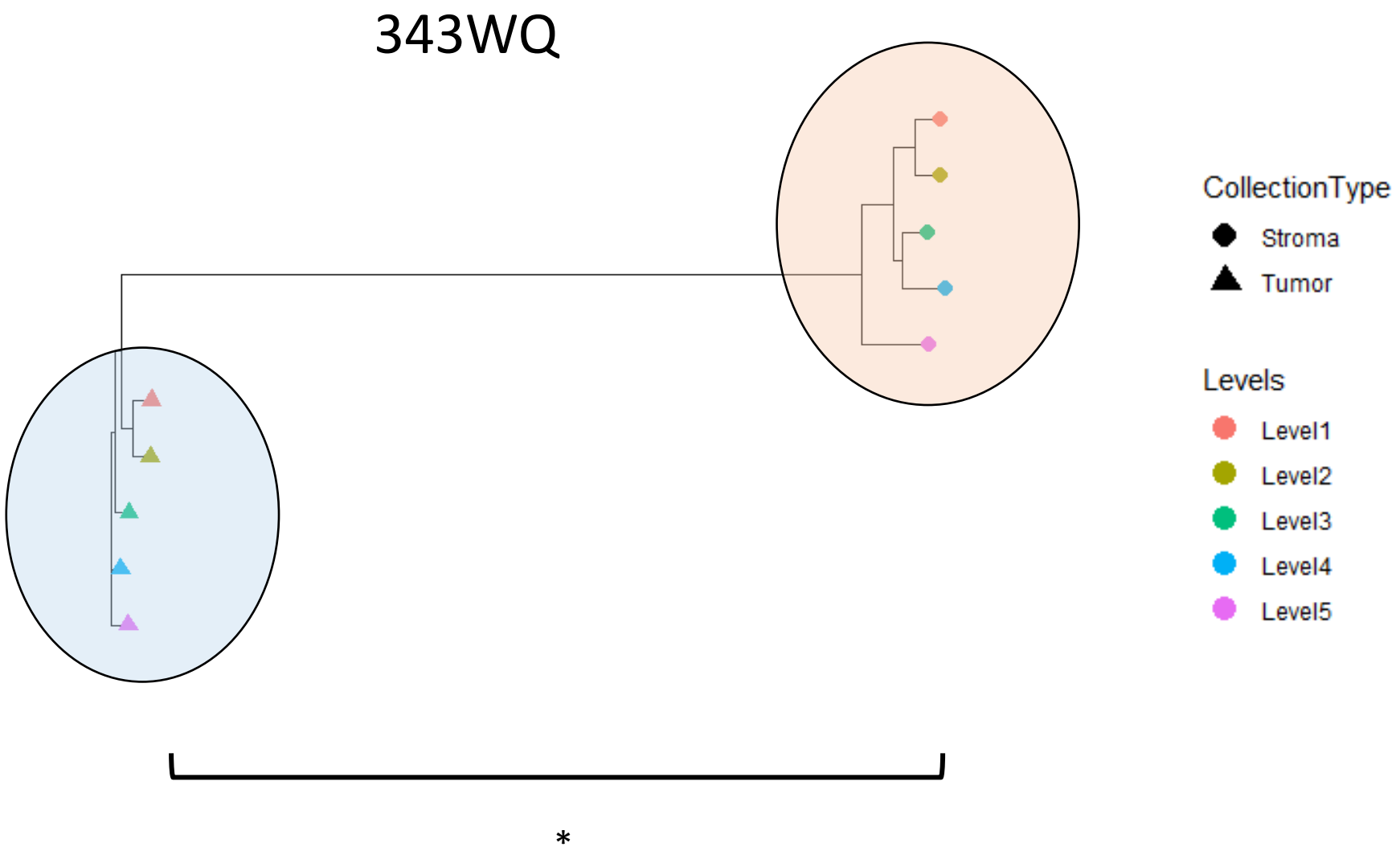
343WQ
CollectionType
Stroma
Tumor
Levels
Level1
Level2
Level3
Level4
Level5
*

Figure 6E

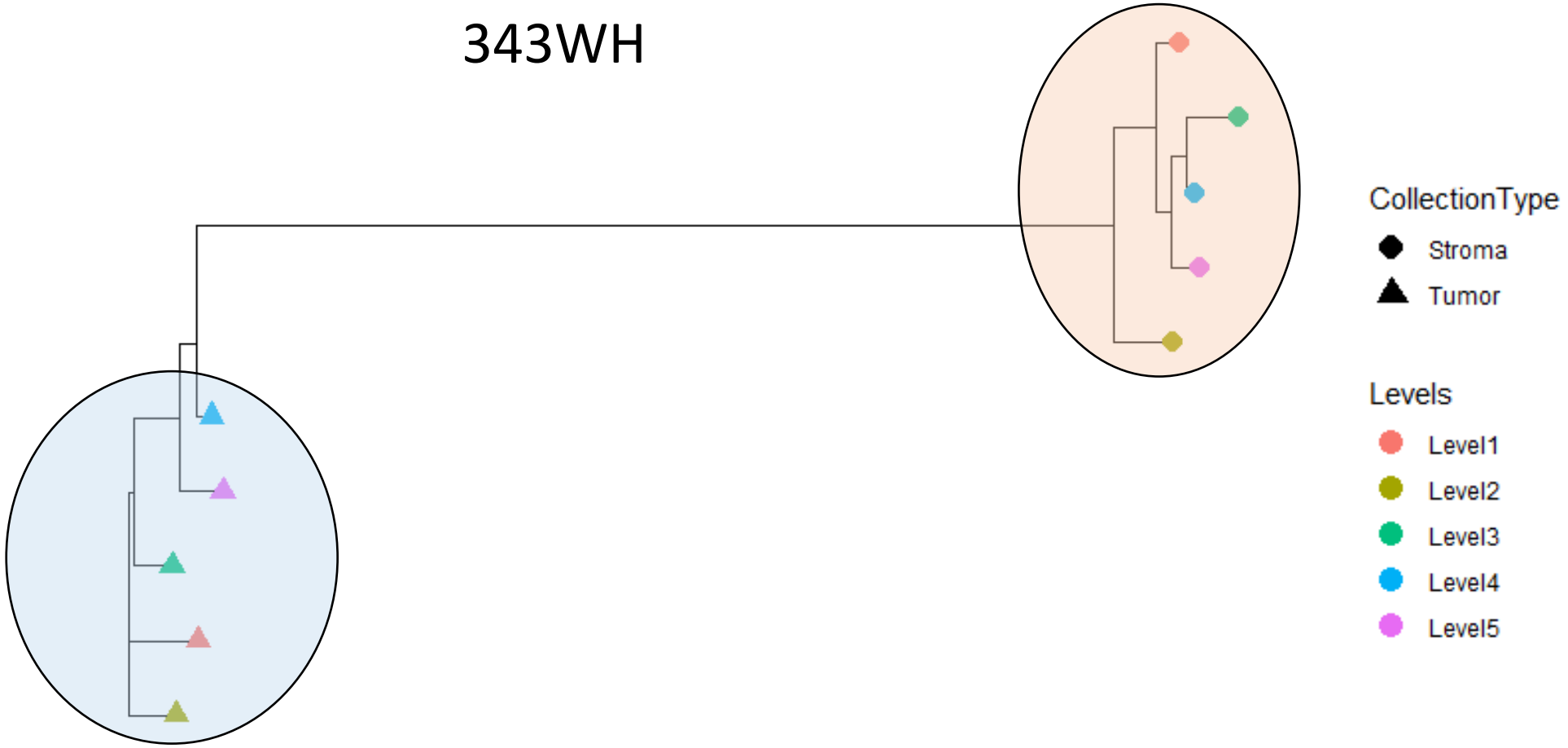
343WH
CollectionType
Stroma
Tumor
Levels
Level1
Level2
Level3
Level4
Level5

Figure 6F

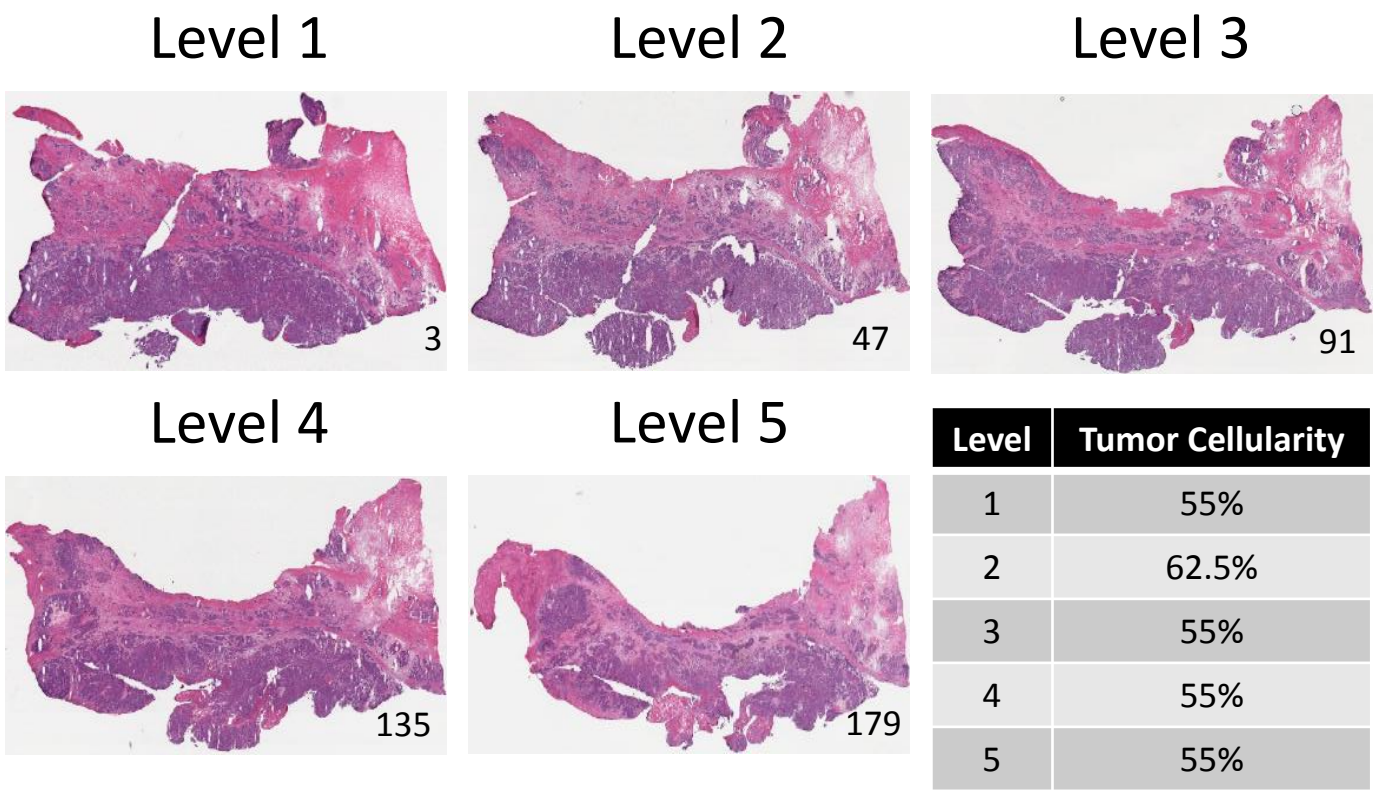

Level	Tumor Cellularity
1	55%
2	62.5%
3	55%
4	55%
5	55%

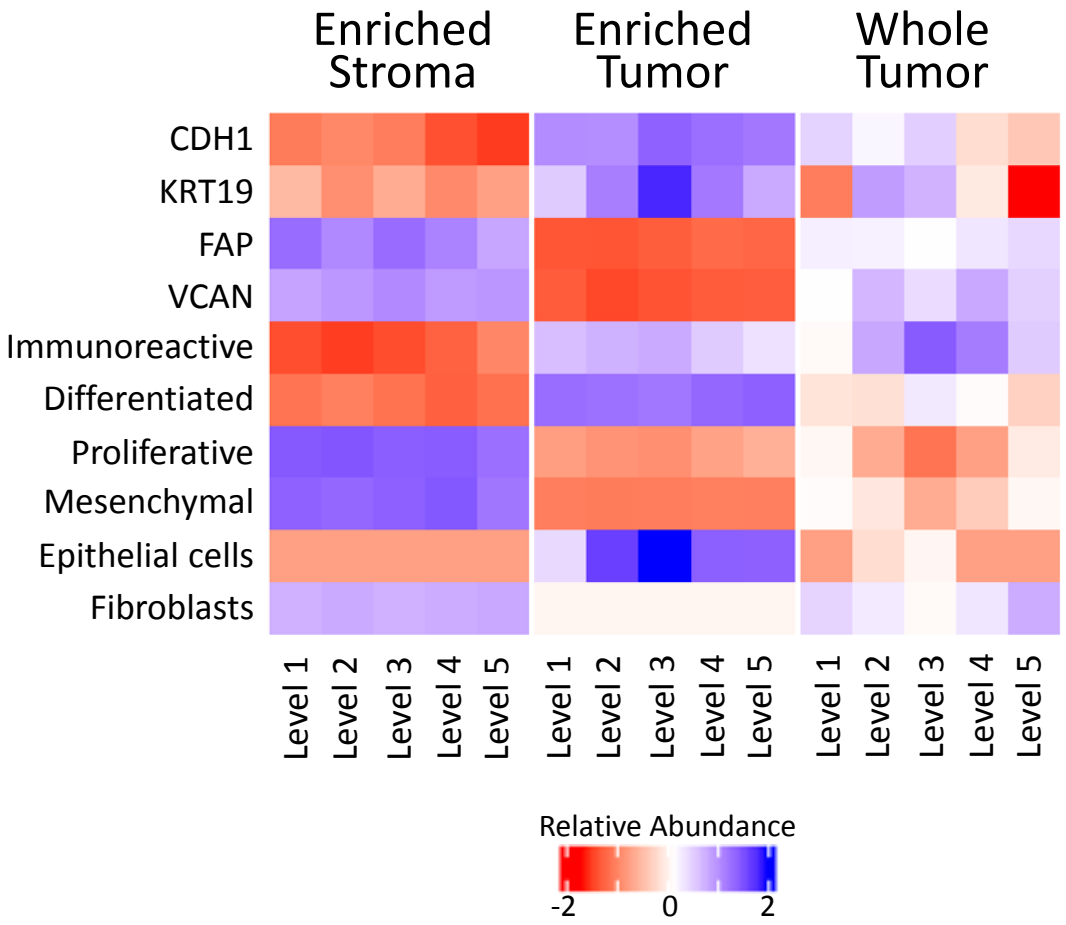

Figure 7

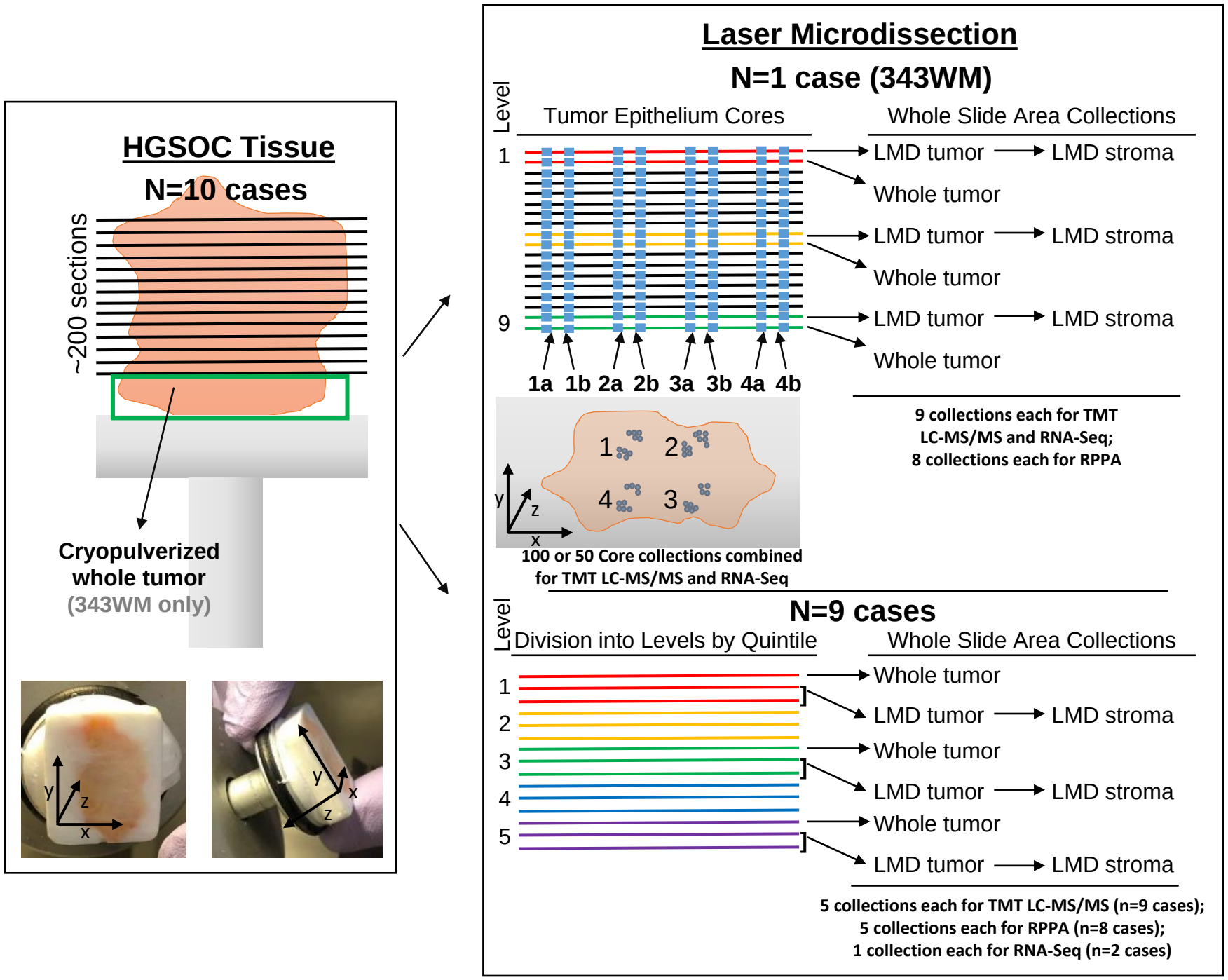

Supplemental Figure 1A

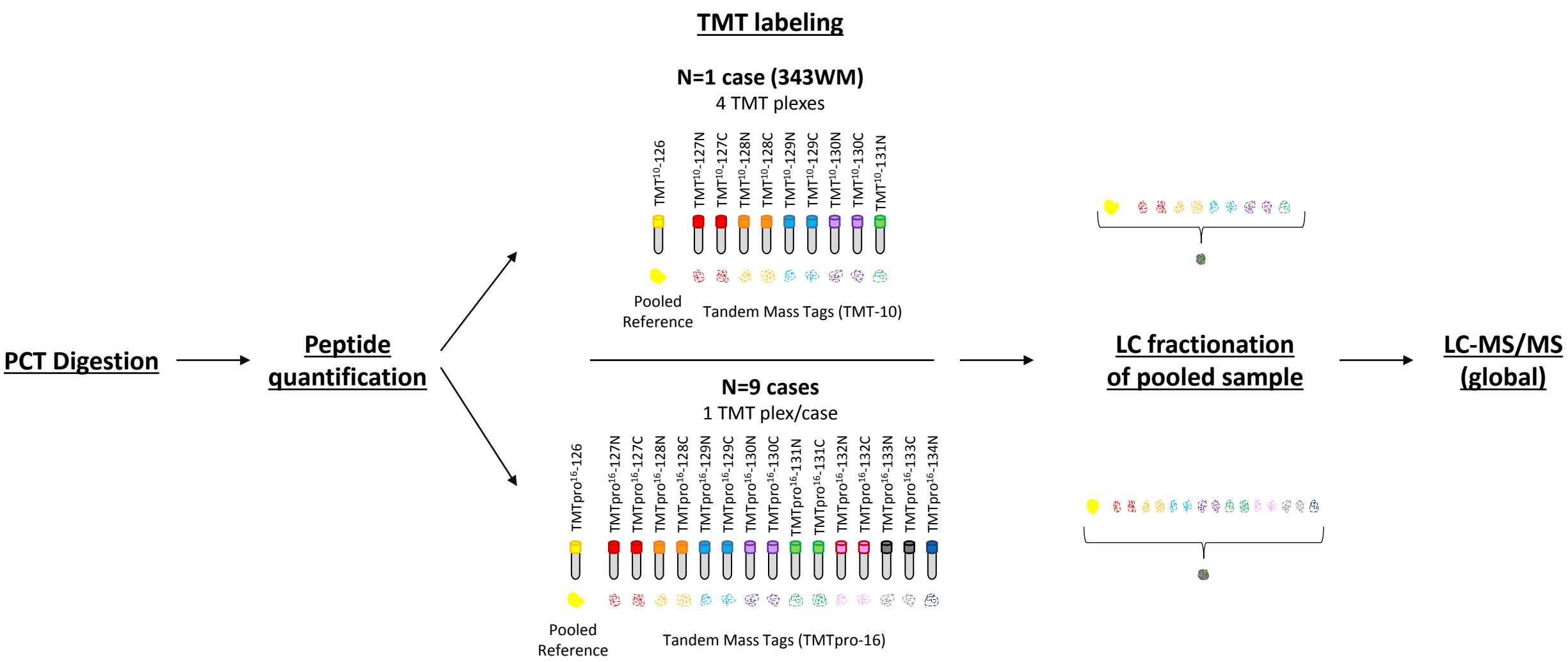

Supplemental Figure 1B

Supplemental Figure 1C

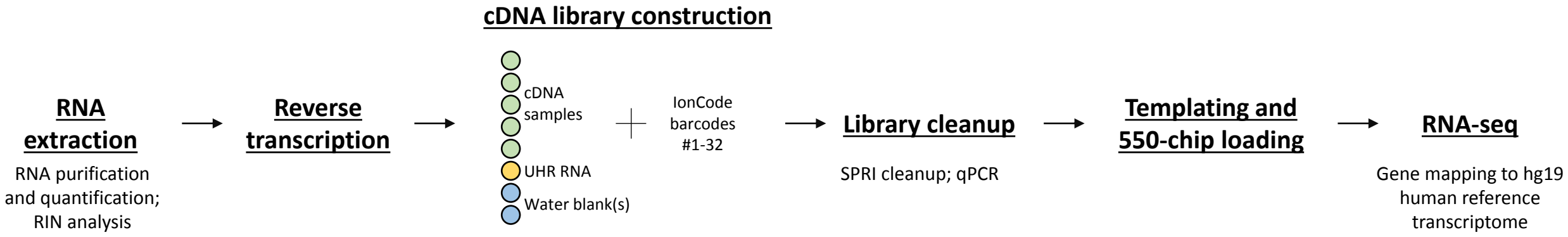

Supplemental Figure 1D

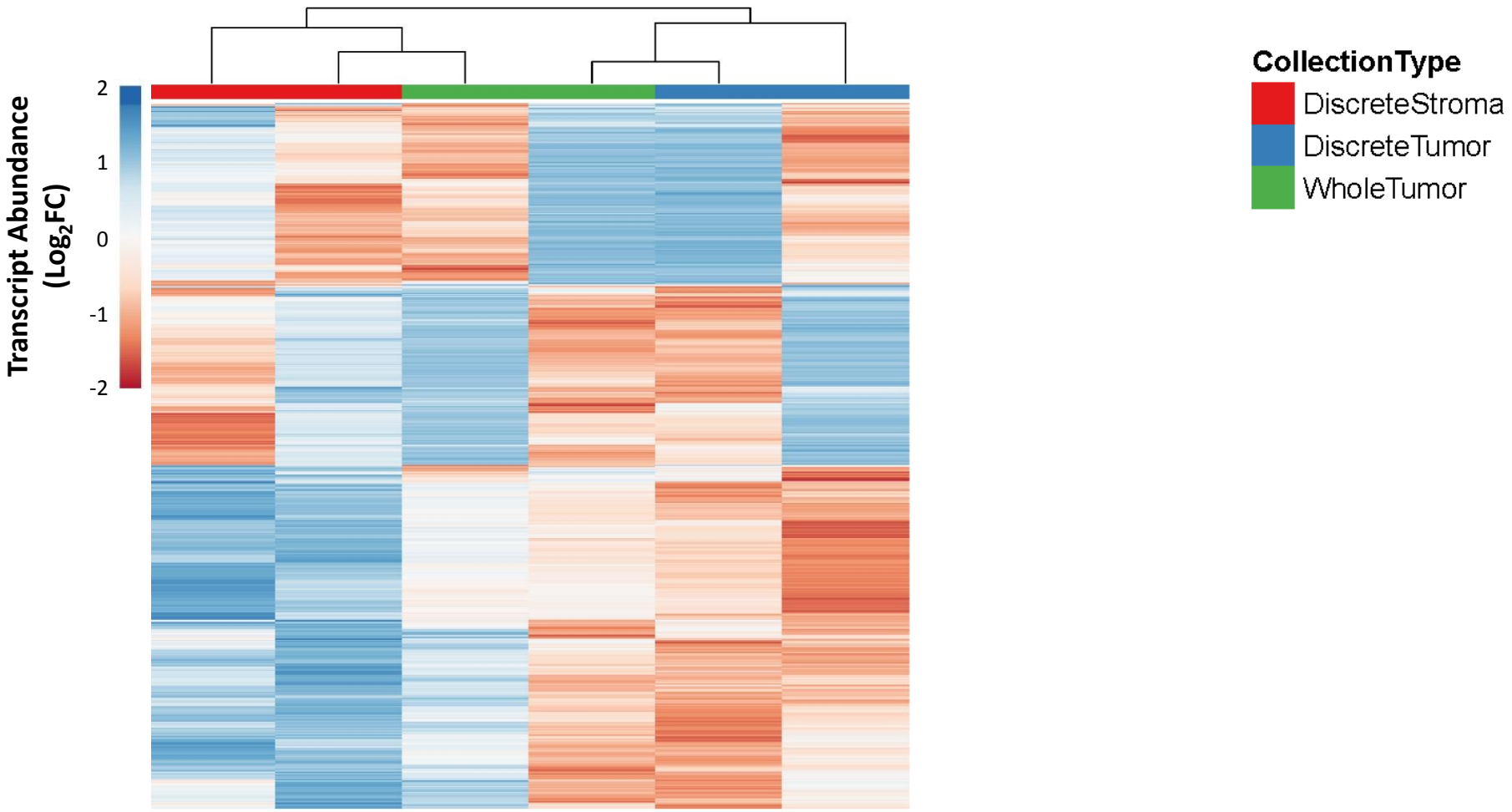

Supplemental Figure 2

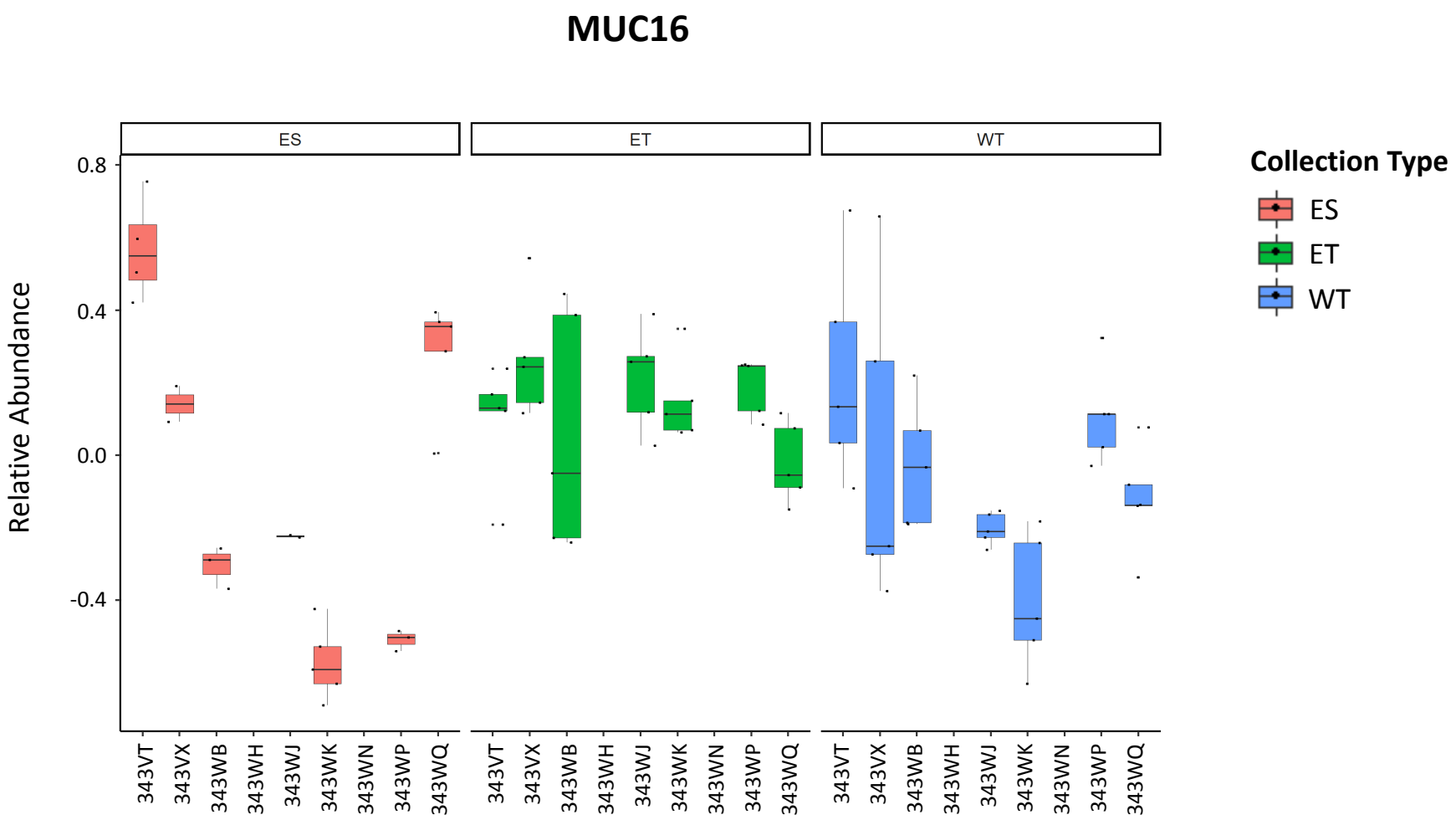

Supplemental Figure 3

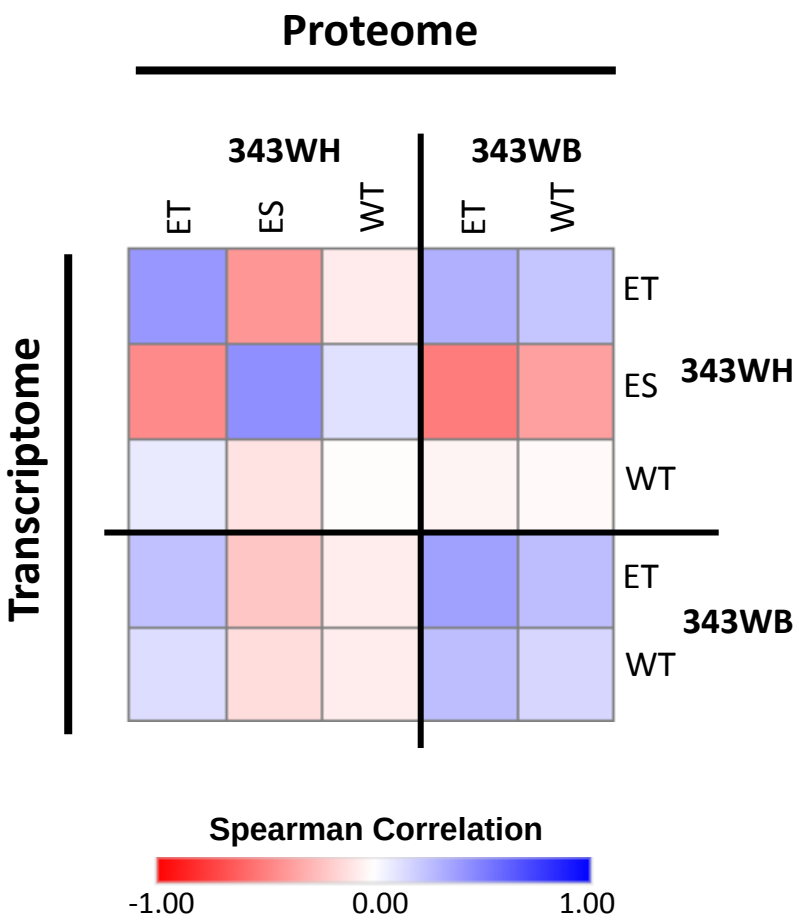

Supplementary Figure 4

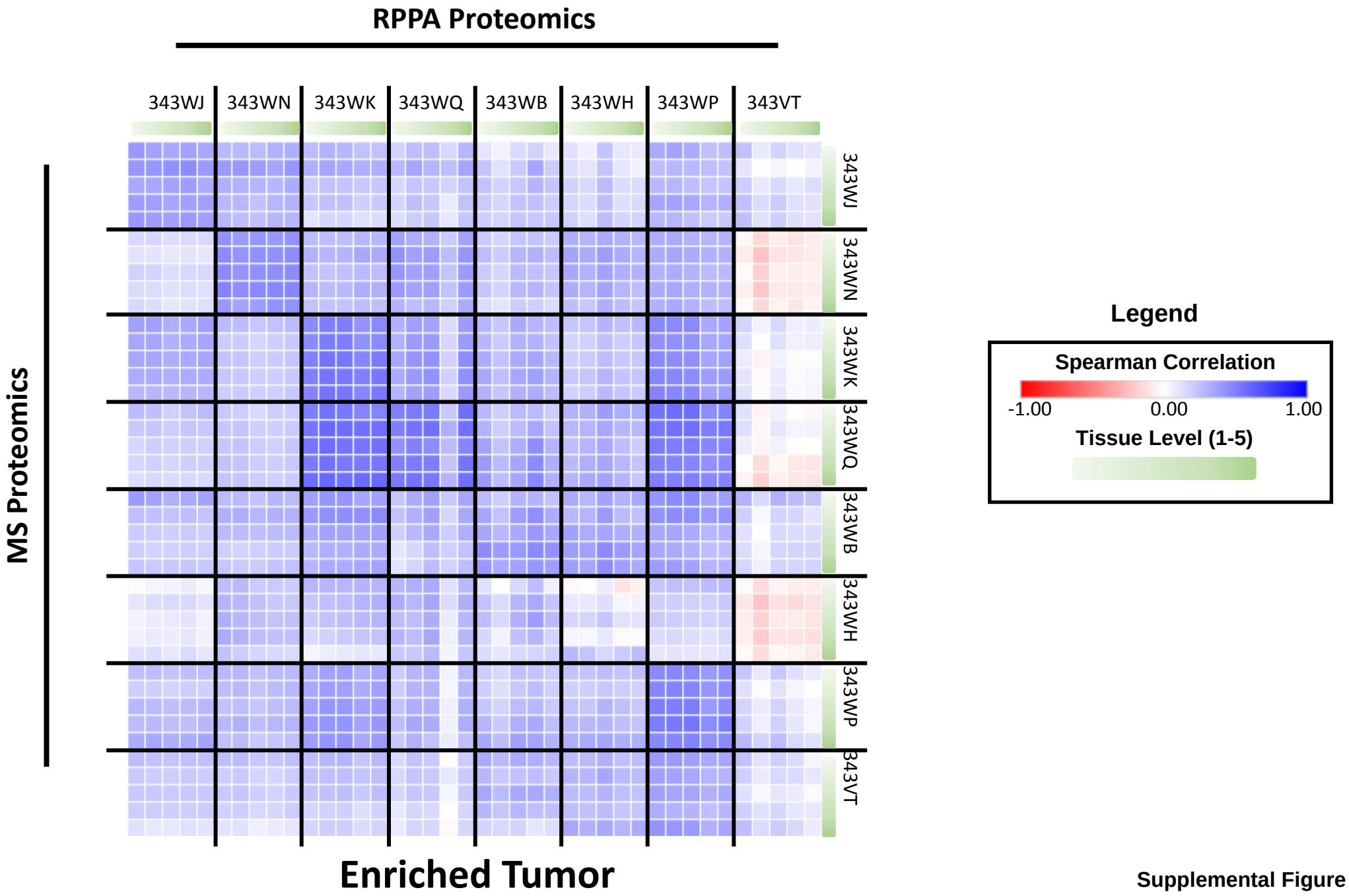

Supplemental Figure 5A

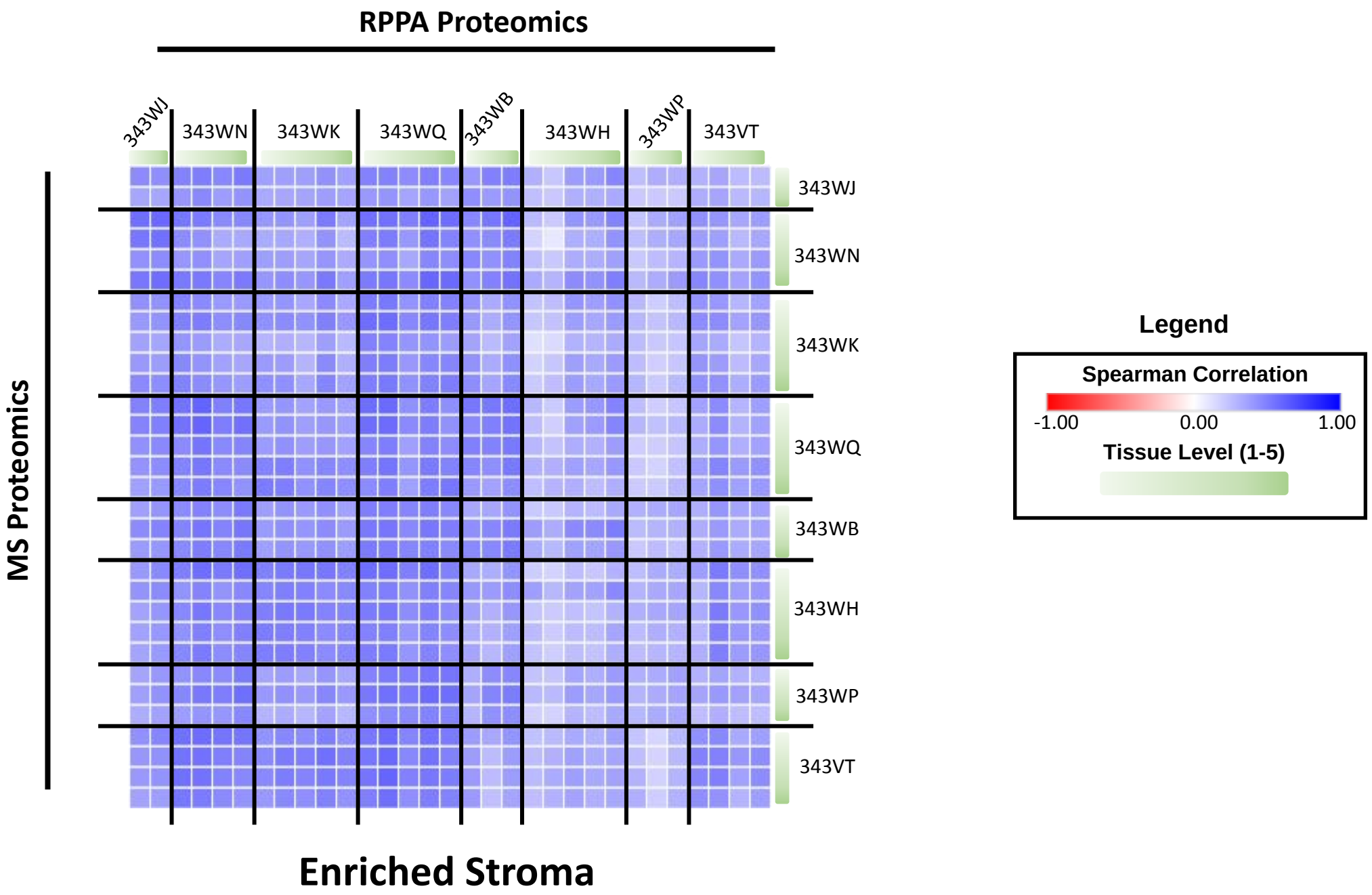

Supplemental Figure 5B

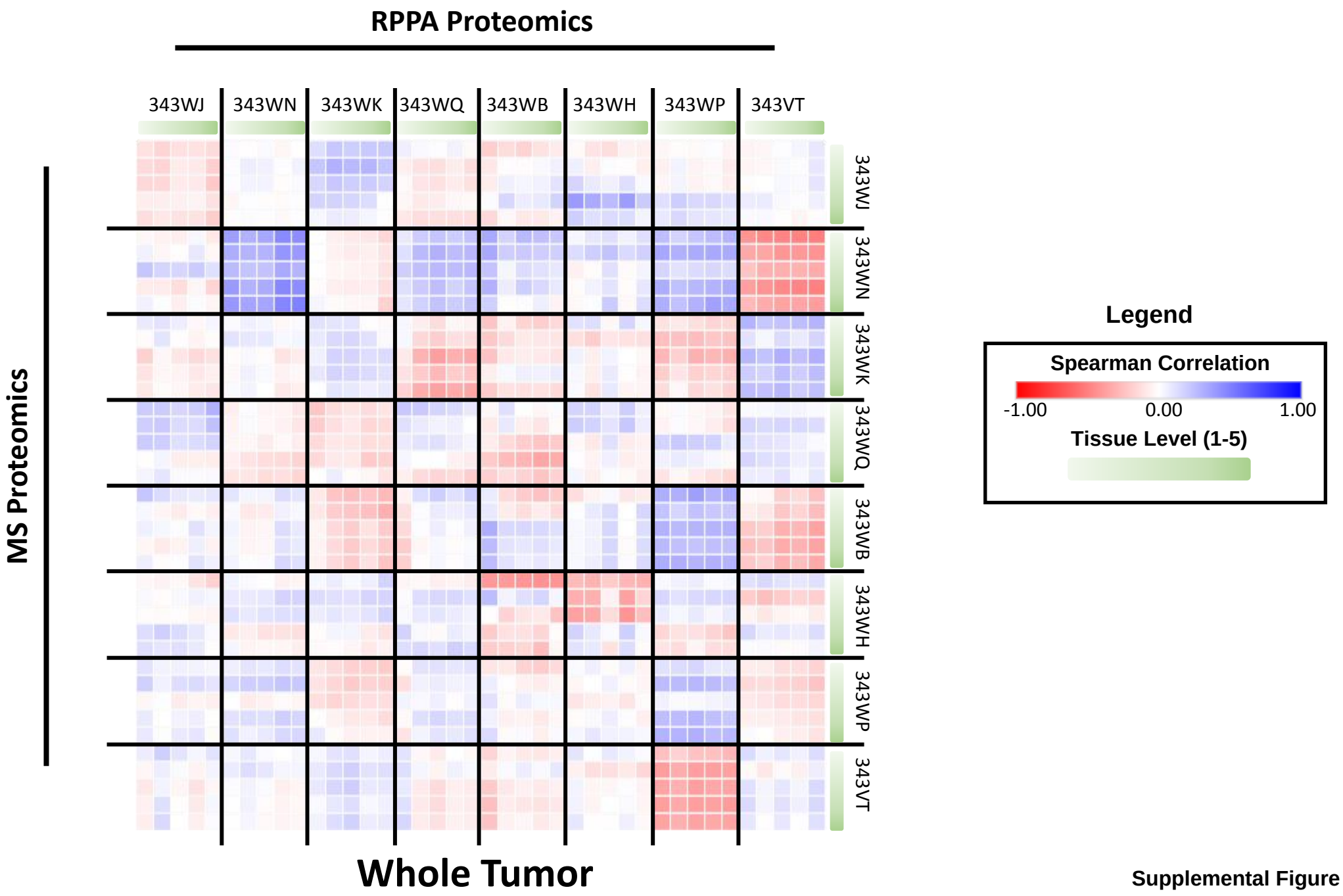

Supplemental Figure 5C

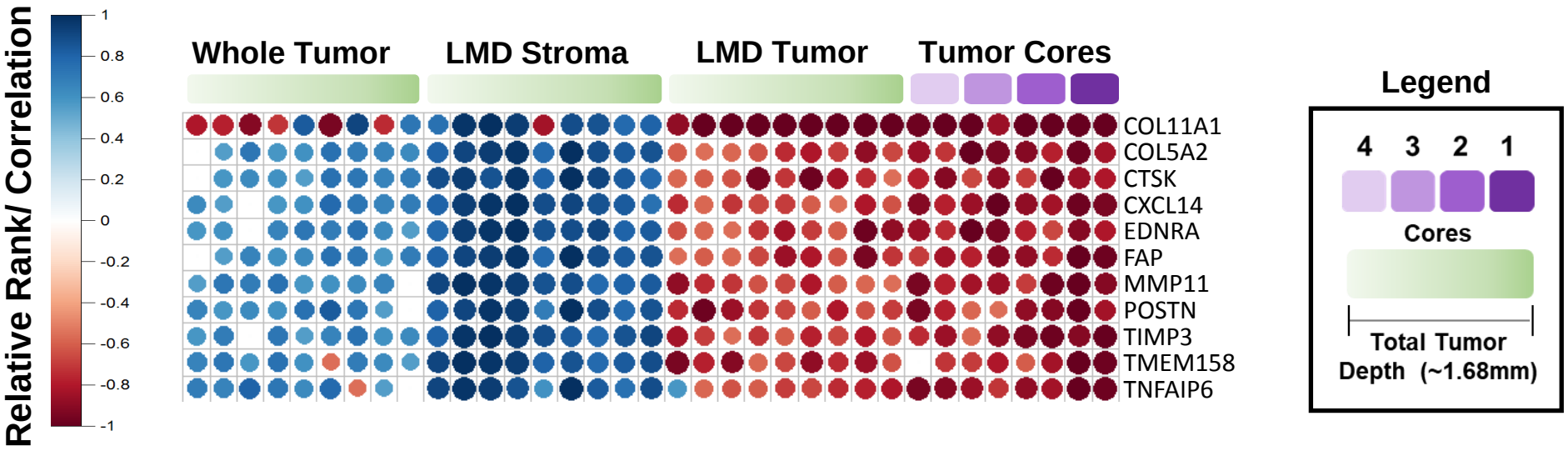

Supplemental Figure 6

343WP: Extremely Sensitive

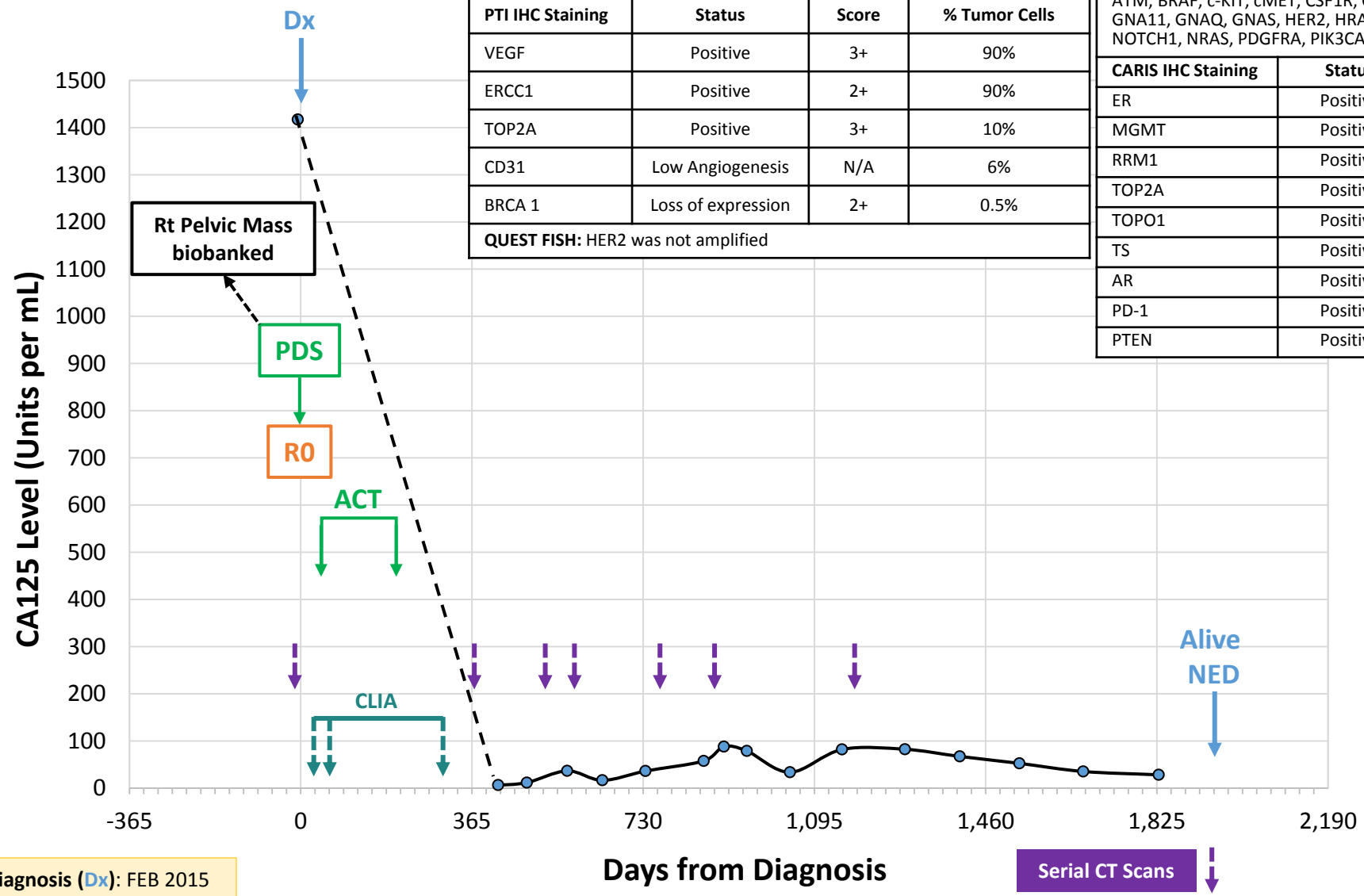

CLIA Test: Run 1-mth after Dx in rt tubo-ovarian tumor from PDS

PRECISION THERAPEUTICS INC (PTI) PCR: Wildtype EGFR, KRAS, BRAF

PTI IHC Staining	Status	Score	% Tumor Cells
VEGF	Positive	3+	90%
ERCC1	Positive	2+	90%
TOP2A	Positive	3+	10%
CD31	Low Angiogenesis	N/A	6%
BRCA 1	Loss of expression	2+	0.5%

QUEST FISH: HER2 was not amplified

CLIA Test: Run 2-mths after Ca Dx in pelvic mass from PDS

CARIS NGS: Pathogenic Mutation detected in TP53 (R342X). No Pathogenic Mutations detected in BRCA1, BRCA2, ABL1, AKT1, ALK, APC, ATM, BRAF, c-KIT, cMET, CSF1R, CTNNB1, EGFR, FGFR1, FGFR2, FLT3, GNA11, GNAQ, GNAS, HER2, HRAS, IDH1, JAK2, VEGFR2, KRAS, MPL, NOTCH1, NRAS, PDGFRA, PIK3CA, PTEN, RET, SMO, VHL

CARIS IHC Staining	Status	Score	% Tumor Cells
ER	Positive	2+	90%
MGMT	Positive	1+	95%
RRM1	Positive	2+	60%
TOP2A	Positive	1+	25%
TOPO1	Positive	2+	60%
TS	Positive	1+	40%
AR	Positive		
PD-1	Positive		
PTEN	Positive		

CLIA Test: Run 8-mths after Dx in saliva

AMBRY GENETICS OvaNext NGS: RAD51C p.V151M Variant of Unknown Significant. No Pathogenic Mutations in the 24 Hereditary Ovarian Cancer Genes including ATM, BARD1, BRCA1, BRCA2, CDH1, CHEK2, EPCAM, MLH1, MRE11A, MSH2, MSH6, MUTYH, NBN, NF1, PALB2, PMS2, PTEN, RAD50, RAD51C, RAD51D, SMARCA4, STK11 or TP53

History at Diagnosis (Dx): 50 year-old post-menopausal married Asian non-smoker with a body mass index of 49.6 who presented with abdominal pain, ascites and pre-op CA125 of 1,417 Units/mL. Patient had 2 live births, 4 pregnancies, a history of hypertension and kidney disease, and three second degree relatives with cancer: esophageal cancer (m.uncle), breast cancer (p.cousin) or lung cancer (m.cousin).

Surgical Procedure: Primary debulking surgery (PDS) was an open total abdominal hysterectomy bilateral salpingo-oophorectomy, omentectomy and peritoneal biopsies.

Cancer Dx: Stage IIIA grade 3 serous tubal carcinoma (rt tube) with a moderate disease distribution and 4.5 L ascites that was optimally resected to no residual disease (R0).

Drug Response Phenotype: Extremely Sensitive

Diagnosis (Dx): FEB 2015

PDS: Primary Debulking Surgery at Day 0 from Dx, right pelvic mass biobanked for research, tubo-ovarian tumor submitted for CLIA test 1 and pelvic mass submitted for CLIA test 2

ACT: Adjuvant Chemotherapy with Paclitaxel and Carboplatin X 1C, followed by Abraxane and Carboplatin X 5C (chemo changed due to allergic reaction to Paclitaxel)

R0: No residual disease

Dx: Cancer diagnosed with PDS

NED: Patient is alive and with no evidence of disease at last contact in June 2020 (1963 days from Dx)

Supplemental Figure 7A

343WN: Moderately Sensitive and Deadly

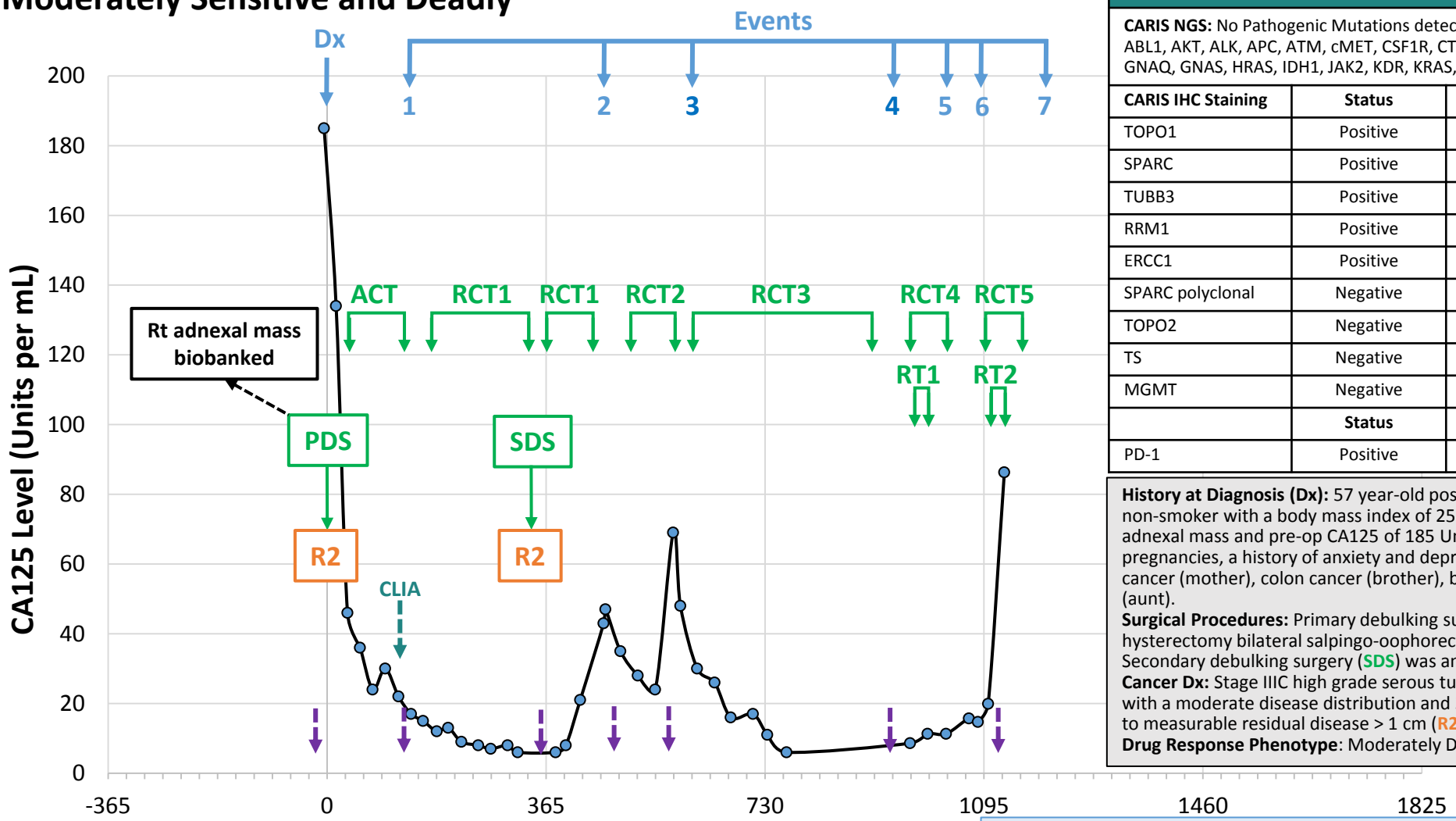

CLIA Test: Run 4-mths after Dx on Epigastric Mass sample collected 105 days after Dx

CARIS NGS: No Pathogenic Mutations detected in BRAF, PIK3CA, c-Kit, PDGFRA, RET, TP53, ABL1, AKT, ALK, APC, ATM, cMET, CSF1R, CTNNB1, EGFR, HER-2, FGFR1, FGFR2, FLT3, GNA11, GNAQ, GNAS, HRAS, IDH1, JAK2, KDR, KRAS, NOTCH1, NRAS, PTEN, SMO, VHL

CARIS IHC Staining	Status	Score	% Tumor Cells
TOPO1	Positive	2+	95%
SPARC	Positive	2+	50%
TUBB3	Positive	3+	95%
RRM1	Positive	2+	90%
ERCC1	Positive	3+	90%
SPARC polyclonal	Negative	0	100%
TOPO2	Negative	0	100%
TS	Negative	0	100%
MGMT	Negative	0	100%
	Status	**Per High Power Field**	
PD-1	Positive	2-5 positive cells	

History at Diagnosis (Dx): 57 year-old post-menopausal married Non-Hispanic White non-smoker with a body mass index of 25.6 who presented with highly suspicious adnexal mass and pre-op CA125 of 185 Units/mL. Patient had 3 live births, 3 pregnancies, a history of anxiety and depression, and four relatives with cancer: rectal cancer (mother), colon cancer (brother), breast cancer (m.aunt) or bladder cancer (aunt).
Surgical Procedures: Primary debulking surgery (PDS) was an open total abdominal hysterectomy bilateral salpingo-oophorectomy, omentectomy and peritoneal biopsies. Secondary debulking surgery (SDS) was an exploratory laparotomy and tumor debulking.
Cancer Dx: Stage IIIC high grade serous tubo-ovarian carcinoma (rt ovary and rt tube) with a moderate disease distribution and 300 mL ascites that was suboptimally resected to measurable residual disease > 1 cm (R2).
Drug Response Phenotype: Moderately Drug Sensitive

PDS: Primary Debulking Surgery on Day 0 from Dx with a persistent R2 retroperitoneal nodal mass, right adnexa biobanked for research
ACT: Adjuvant Chemotherapy with Paclitaxel and Carboplatin
RCT1: Recurrent Chemotherapy 1 with Carboplatin and Gemcitabine before and after SDS X 12C total
SDS: Secondary Debulking Surgery at Day 343 from Diagnosis
RCT2: Recurrent Chemotherapy 2 with Doxorubicin and Bevacizumab
RCT3: Recurrent Chemotherapy 3 with Abraxane and Bevacizumab X 13C
RCT4: Recurrent Chemotherapy 4 with Topotecan
RT1: Radiation Therapy 1 with External Beam concurrent with RCT 4 with Topotecan
RCT5: Recurrent Chemotherapy 5 with Cisplatin
RT2: Radiation Therapy 2 with CyberKnife Stereotactic Body Radiotherapy

Diagnosis (Dx): MAY 2014

R2: Suboptimal residual disease ≥ 1.0 cm

Serial CT Scans

Dx: Cancer diagnosed with a preop CT showing right adnexal complex cystic and solid mass, likely primary ovarian carcinoma with peritoneal tumor implants and bulky peritoneal adenopathy
Event 1: Disease progression seen with CT guided biopsy of upper abdominal mass with pathology showing metastatic poorly differentiated carcinoma Then bone scan showing L1 metastasis
Event 2: Progression seen with CT showing multiple new peritoneal implants
Event 3: Progression seen with CT showing enlargement of hepatic capsular metastasis
Event 4: Progression seen with CT showing interval mixed changes of hepatic metastases redemonstration of peritoneal implants in the abdomen and pelvis overall slightly progressed and progression of destructive lesion involving L1 vertebra
Event 5: Patient underwent spinal surgery for progressive metastatic carcinoma lesion on L1
Event 6: Progression seen with MRI showing new widespread hepatic metastases and mild progression of the subcutaneous and peritoneal metastases and CT guided biopsy of liver with pathology showing metastatic poorly differentiated adenocarcinoma
Event 7: Cancer related death at Day 1169 from Diagnosis

Supplemental Figure 7B

343WQ: Aggressive, Resistant and Deadly

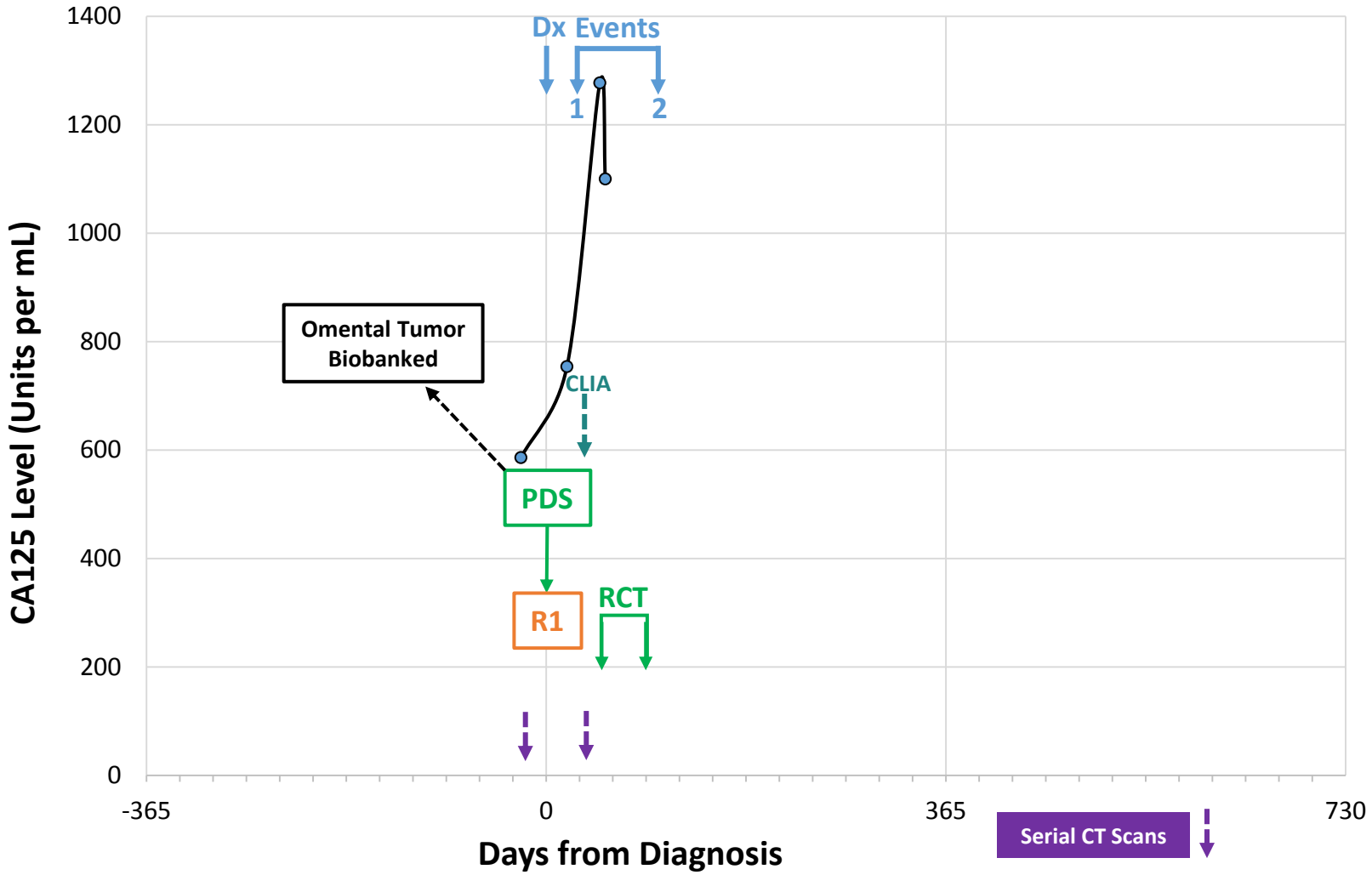

Diagnosis (Dx): JUL 2015

PDS: Primary Debulking Surgery at Day 0 from Dx, omental tumor biobanked
RCT: Recurrent Chemotherapy with Paclitaxel and Carboplatin X 1C

R1: Macroscopic residual disease < 1.0 cm

Dx: Cancer diagnosed with PDS
Event 1: Progression seen with CT and MRI showing redemonstrations of large intraabdominal ascites and biopsy of the ampulla with pathology showing metastatic high grade serous carcinoma and paracentesis with cytology positive for rare malignant cells
Event 2: Cancer related death at Day 81 from Diagnosis

CLIA Test: Caris Testing Run 8/2015 on Iliac lymph node sample collected at PDS, Day 0 from Diagnosis

CARIS NGS: Presumed Pathogenic Mutation detected in TP53 Exon 8 (R267P). No Pathogenic Mutations detected in BRCA1, BRCA2, ABL1, AKT1, ALK, APC, ATM, BRAF, c-KIT, cMET, CSF1R, CTNNB1, EGFR, FGFR1, FGFR2, FLT3, GNA11, GNAQ, GNAS, HER2, HRAS, IDH1, JAK2, VEGFR2, KRAS, MPL, NOTCH1, NRAS, PDGFRA, PIK3CA, PTEN, RET, SMO, VHL

CARIS IHC Staining	Status	Score	% Tumor Cells
ERCC1	Negative	2+	20%
ALK	Positive	3+	1%
Her2/Neu	Negative	2+	1%
PGP	Negative	0	100%
TOP2A	Positive	1+	15%
TOPO1	Positive	2+	30%
ER	Negative	0	100%
PR	Negative	0	100%
TS	Positive	1+	10%
MGMT	Positive	1+	100%
PGP	Negative	0	100%
TUBB3	Positive	2+	100%

History at Diagnosis (Dx): 66 year-old post-menopausal married Caucasian former smoker for 40 years with a body mass index of 32.9 who presented with adnexal mass, ascites, lymphadenopathy and pre-op CA125 of 586 Units/mL. Patient had 0 pregnancies, a history of hypercholesterolemia and anxiety, and no biologic relatives with cancer.
Surgical Procedure: Primary debulking surgery (**PDS**) was a laparoscopic procedure that converted to an open total abdominal hysterectomy, bilateral salpingo-oophorectomy, omentectomy, peritoneal biopsies, and pelvic lymphadenectomy.
Cancer Dx: Stage IIIC HG Serous Carcinoma of the Ovary that was optimally resected to macroscopic residual disease < 1 cm (**R1**).
Drug Response Phenotype: Drug Resistant

Supplemental Figure 7B